Remote Sensing of Environment 114 (2010) 1610–1627

Contents lists available at ScienceDirect

Remote Sensing of Environment

journal homepage: www.elsevier.com/locate/rse

Retrieving vegetation height of forests and woodlands over mountainous areas in the Pacific Coast region using satellite laser altimetry

Qi Chen *

Department of Geography, University of Hawai`i at Mānoa, 422 Saunders Hall, 2424 Maile Way, Honolulu, HI, 96822, USA

ARTICLE INFO

Article history:
Received 23 October 2009
Received in revised form 19 February 2010
Accepted 21 February 2010

Keywords:
GLAS
Vegetation height
Mountain
Conifer
Woodland
Airborne lidar
Mixed-effects model

ABSTRACT

The challenge to retrieve canopy height from large-footprint satellite lidar waveforms over mountainous areas is formidable given the complex interaction of terrain and vegetation. This study explores the potential of GLAS (Geoscience Laser Altimeter System) for retrieving maximum canopy height over mountainous areas in the Pacific Coast region, including two conifers sites of tall and closed canopy and one broadleaf woodland site of shorter and sparse canopy. Both direct methods and statistical models are developed and tested using spatially extensive coincident airborne lidar data. The major findings include: 1) the direct methods tend to overestimate the canopy height and are complicated by the identification of waveform signal start and terrain ground elevation, 2) the exploratory data analysis indicates that the edge-extent linear regression models have better generalizability than the edge-extent nonlinear models at the inter-site level, 3) the inter-site level test with mixed-effects models reveals that the edge-extent linear models have statistically-justified generalizability between the two conifer sites but not between the conifer and woodland sites, 4) the intra-site level test indicates that the edge-extent linear models have statistically-justified generalizability across different vegetation community types within any given site; this, combined with 3), unveils that the statistical modeling of maximum canopy height over large areas with edge-extent linear models only need to consider broad vegetation differences (such as woodlands versus conifer forests instead of different vegetation communities within woodlands or conifer forests), and 5) the simulations indicate that the errors and uncertainty in canopy height estimation can be significantly reduced by decreasing the footprint size. It is recommended that the footprint size of the next-generation satellite lidar systems be at least 10 m or so if we want to achieve meter-level accuracy of maximum canopy height estimation using direct and statistical methods.

1. Introduction

The vegetation in the Pacific Coast region provides important goods and ecological services. The Pacific Coast forests, located in Northern California, Oregon, and Washington, cover approximately 200,000 km^2 and are the most productive forest region in the United States, producing 25% of the annual lumber and 75% of the plywood in the United States (Sharpe et al., 2003). These forests are typically coniferous, closed, and tall, including 100-m-tall redwoods and giant sequoias that may reach 10 m in diameter. Woodlands are another major type of vegetation in this region that mostly grows in California. Contrary to the coastal conifer forests, woodlands are deciduous, more open, and shorter. Nevertheless, they have important ecological functions in protecting the soils in the Sierra Nevada and Coastal mountain ranges and providing water for California's multi-billion dollar agricultural economy (Baldocchi et al., submitted for publication). It is expected that remote sensing can provide useful vegetation information for sustainable ecosystem management over this region.

Vegetation height is one of the leading dimensions of ecological variations among tree species (Westoby et al., 2002) and is central to ecosystem functioning (Moles et al., 2009). This study investigates the potential of satellite laser altimetry, specifically the GLAS (Geoscience Laser Altimeter System) on board ICESat (Ice, Cloud,and land Elevation Satellite), for retrieving vegetation height of Pacific Coast forests and woodlands. The lasers on GLAS transmit pulses from an altitude of ~600 km, producing 60 m nominal footprint size and ~170 m shot-spacing on the ground (Zwally et al., 2002; Chen, 2010). The receiver on GLAS records the vertical canopy structure up to 81.6 m for the early laser campaigns (Laser 1a and 2a periods) or 150 m for the later campaigns to avoid truncation of signals from tall objects or steep slope (Harding & Carabajal, 2005). The waveforms of 81.6 m have a vertical resolution of 15 cm for a total of 544 bins while the waveforms of 150 m have a vertical resolution of 15 cm for the lower 392 bins and 60 cm for the upper 152 bins. Since its launch in 2003, GLAS has produced unprecedented dataset at the global scale (Harding & Carabajal 2005). Nevertheless, only a paucity of studies

* Tel.: +1 808 956 3524; fax: +1 808 956 3512.
E-mail address: qichen@hawaii.edu.

0034-4257/$ – see front matter © 2010 Elsevier Inc. All rights reserved.
doi:10.1016/j.rse.2010.02.016

has explored the use of GLAS for vegetation height retrieval (Lefsky et al., 2005; Lefsky et al., 2007; Duong et al., 2008; Neuenschwander et al., 2008; Rosette et al., 2008; Sun et al., 2008; Pang et al., 2008; Duncanson et al., 2010).

The previous studies have used either direct (Duong et al., 2008; Neuenschwander et al., 2008; Sun et al., 2008) or statistical (Lefsky et al., 2005; Lefsky et al., 2007; Rosette et al., 2008; Pang et al., 2008; Duncanson et al., 2010) methods to extract canopy height from GLAS data. A GLAS waveform is typically characterized by multiple energy peaks caused by the reflection from ground surface and the objects (e.g. trees) above it (Fig. 1). Over flat areas, the lowest peak usually corresponds to the ground if there is enough energy penetrating through the surface objects. The direct methods are to simply estimate canopy height based on the vertical difference between the waveform signal start, which assumes to be the canopy top, and the ground peak (Fig. 1(a)) (Hofton et al., 2000; Neuenschwander et al., 2008). To find the ground peak, Gaussian decomposition is usually used to decompose each waveform into multiple Gaussian distributions, assuming the lowest peak representing the ground elevation (Hofton et al., 2000; Duong et al., 2008; Neuenschwander et al., 2008). The direct methods work well over flat areas (Neuenschwander et al., 2008). However, over mountainous areas with large relief and complex terrain, the peaks from ground and surface objects can be broadened and mixed, making the identification of ground elevation difficult (Zwally et al., 2002; Harding & Carabajal, 2005; Lefsky et al., 2005; Chen, 2010). Over complex terrain, the lowest peak might correspond to objects (e.g. short trees at the lower side of a footprint) or minor terrain features that do not represent the central tendency of terrain elevation within a footprint (e.g., flat surface such as waters and valleys passing through the footprints). Several studies have found that the elevation of the stronger one among the lowest two Gaussian peaks, z_{mp}, might have a better correspondence to ground elevation (Rosette et al., 2008; Chen, 2010). Rosette et al. (2008) used z_{mp} to calculate canopy height from GLAS data and found that it has better correlation with field measurements of canopy height than using the lowest peak for 19 shots over a woodland in Gloucestershire, UK. Chen (2010) analyzed ~500 shots over a ~2000 km^2 region in North Carolina and found that z_{mp} is the best metric for ground

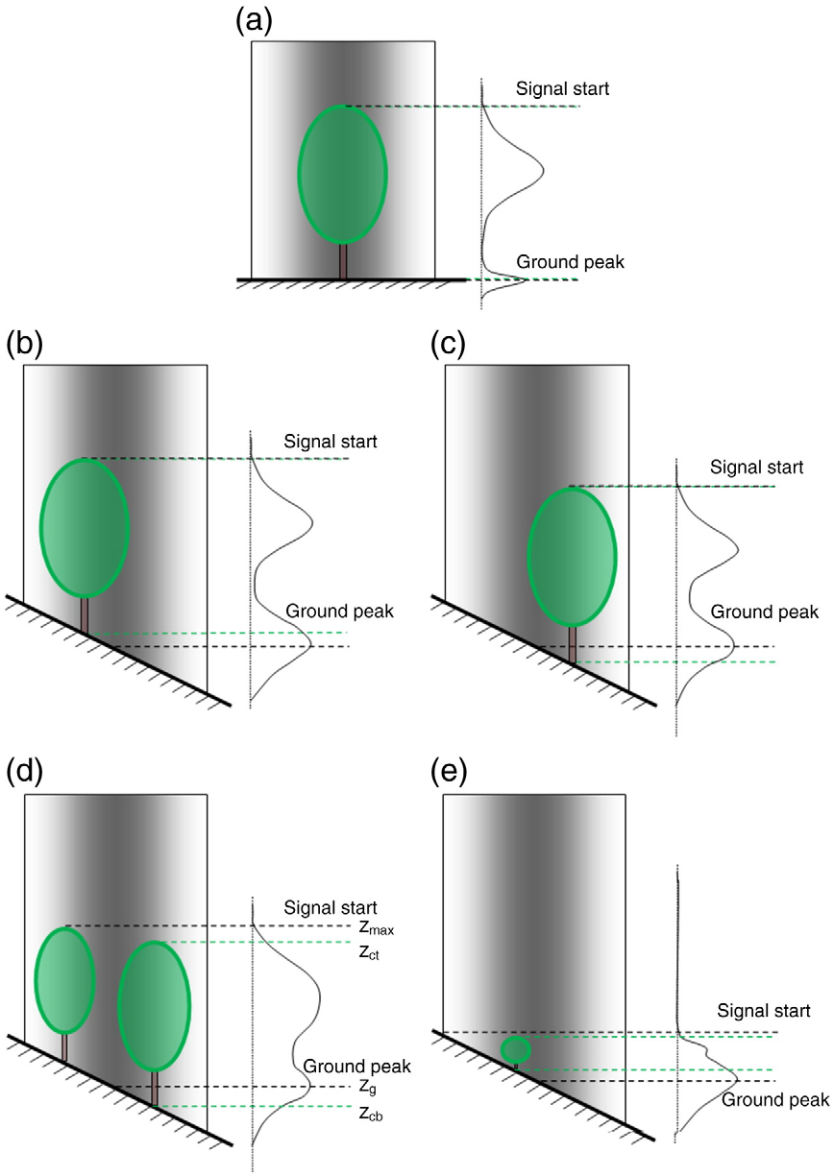

Fig. 1. Scenarios to illustrate the effects of terrain slope and plant size and distribution on canopy height estimation. (a) a plant over a flat surface; (b) a plant over a sloped surface and plant bottom is above ground peak; (c) a plant over a sloped surface and plant bottom is below ground peak; (d) plants over a sloped surface but top of the tallest tree (z_{ct}) is below the maximum elevation (z_{max}); (e) a short plant over a sloped surface with the maximum ground elevation is higher than the canopy top elevation.

elevation over both open terrain (with a bias of 0 ± 0.77 m) and mountainous forest areas (with a bias of 0.38 ± 7.02 m). Even if the terrain is simple with approximately constant slope, a non-flat terrain might cause canopy height to be overestimated or underestimated, depending on the spatial distribution of plants within footprints (see Fig. 1(b) and (c)). To my best knowledge, no research has been done to explore these research questions: Will direct methods over- or under-estimate canopy height on average? What are their error sources? How can the errors be minimized?

Besides the direct methods, statistical regression methods have been developed to predict canopy height with waveform metrics. The regression models typically include waveform extent (Lefsky et al., 2005; Rosette et al., 2008), which is the vertical distance between the signal start and end of a waveform. Generally, the waveform extent will increase with terrain slope even if the canopy is the same. Therefore, metrics related to terrain slope are needed in the regression models to remove its effects. The terrain information can be derived from ancillary DEMs (Digital Elevation Models) (Lefsky et al., 2005; Rosette et al., 2008) or from the waveform itself based on metrics such as leading and trailing edge extent (Lefsky et al., 2007; Pang et al., 2008). Unlike the direct methods, the statistical models are essentially site-specific. Therefore, it is critical to investigate the model generalizability over sites with different vegetation and terrain conditions. In the past, statistical models have been developed and tested with a focus on forest areas with dense canopy (Lefsky et al., 2007; Rosette et al., 2008; Pang et al., 2008) and little research has been done over open and sparse canopy such as woodlands, especially over mountainous areas. The difficulty of measuring open and short vegetation using GLAS has been demonstrated in a recent study by Nelson (in press). He compared the canopy height from airborne profiling lidar and GLAS over 272 shots distributed between 46°N and 80°N in Quebec, Canada. The airborne profiler canopy height was calculated as the average height of laser pulses on any given GLAS shot. The GLAS canopy height was calculated as the vertical location of the waveform above the ground peak where 50% of the waveform energy lies above the height and 50% below. It was found that GLAS overestimated the tree height up to 8 m over the treeline where airborne profiler canopy heights are zeros.

When large-footprint waveform lidar systems acquire data over mountainous vegetation areas, it is very likely to have terrain and canopy returns at the same elevation, which makes the extraction of terrain and vegetation information complicated and challenging (Hyde et al., 2005; Chen, 2010). Therefore, the main objectives of this study are to examine 1) how canopy height can be estimated from GLAS data over mountainous areas using both direct and statistical methods, 2) how a specific method can be applied across different vegetation types including forests and woodlands, and 3) what the error sources are when direct methods are used to estimate canopy

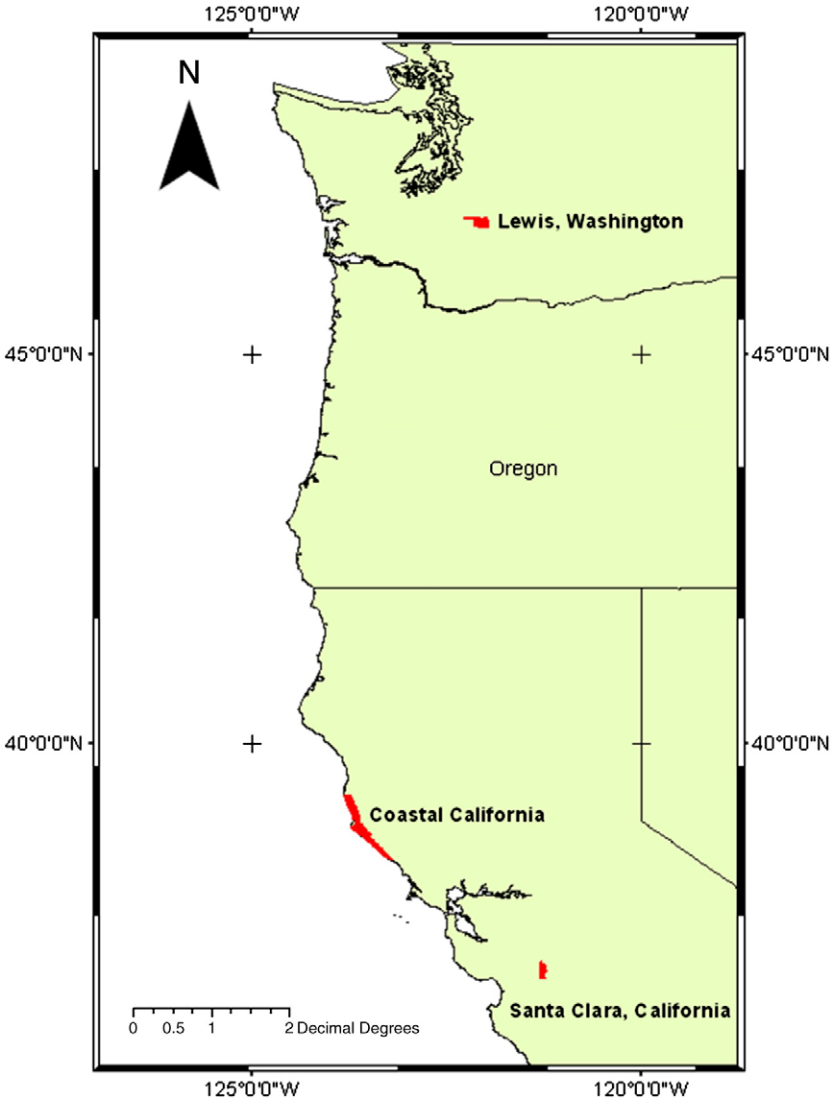

Fig. 2. Locations of the three study sites (Mendocino, California; Santa Clara, California; Lewis, Washington).

height and how these errors can be minimized. As a state-of-the-art remote sensing technology to measure 3D vegetation and terrain properties precisely over large areas (Chen et al., 2007b; Chen, 2007; Pang et al., 2008; Chen, 2010), airborne lidar is used to derive an accurate and spatially-extensive dataset of canopy height and terrain elevation over each GLAS footprint to evaluate different methods. Given the importance of maximum canopy height in plant ecology (e.g., Moles et al., 2009) and biomass mapping (e.g., Lefsky et al., 2005; Boudreau et al., 2008), this study focuses on the estimation of maximum canopy height within footprints from GLAS data.

2. Study area and data

2.1. Study area

The study area covers three mountainous vegetated sites, including one conifer forest site in Mendocino, California, one woodland site in Santa Clara, California, and another conifer forest site in Lewis, Washington (Fig. 2). The Mendocino site is located in the northern San Andreas Fault. Its primary land cover is upland redwood forest, with a minority of pygmy cypress dwarf woodland and northern mixed chaparral in the southeast and Bishop pine forest along the coast and the valley (Fig. 3(a)). The major co-dominant species for primary land covers are Coast Redwood (*Sequoia sempervirens*) and Douglas Fir (*Pseudotsuga menziesii*) for upland redwood forest, non-native annual grassland (*Avena* spp., *Bromus* spp., *etc.*) and Bishop Pine (*Pinus muricata*) for Bishop pine forest, and Eastwood Manzanita (*Arctostaphylos glandulosa*) and Littleberry Manzanita (*Arctostaphylos nummularia*) for northern mixed chaparral and pygmy cypress dwarf woodland and Littleberry Manzanita (Table 1(a)).

The primary land covers in the Santa Clara site are coast live oak forest, blue oak woodland, and California annual grassland, with a minority of Scrubs, Chaparral, and mixed evergreen forest (Fig. 3(b)). The co-dominant species for coast live oak forest are Blue Oak (*Quercus douglasii*) and Coast Live Oak (*Quercus agrifolia*) (Table 1(b)). The blue oak woodland is composed of Blue Oak, Valley Oak (*Quercus lobata*), Buckeye (*Aesculus californica*), and non-native annual grassland. There are also a minority of Diablan sage scrub, composed of California Sagebrush (*Artemisia californica*) and non-native annual grassland, and mixed evergreen forest, composed of Coast Live Oak and California Bay (*Umbellularia californica*) (Table 1(b)).

The Lewis site mainly consists of conifer forests in the mid-seral stage as well as in the early- and late-seral stages (Fig. 3(c)). In the

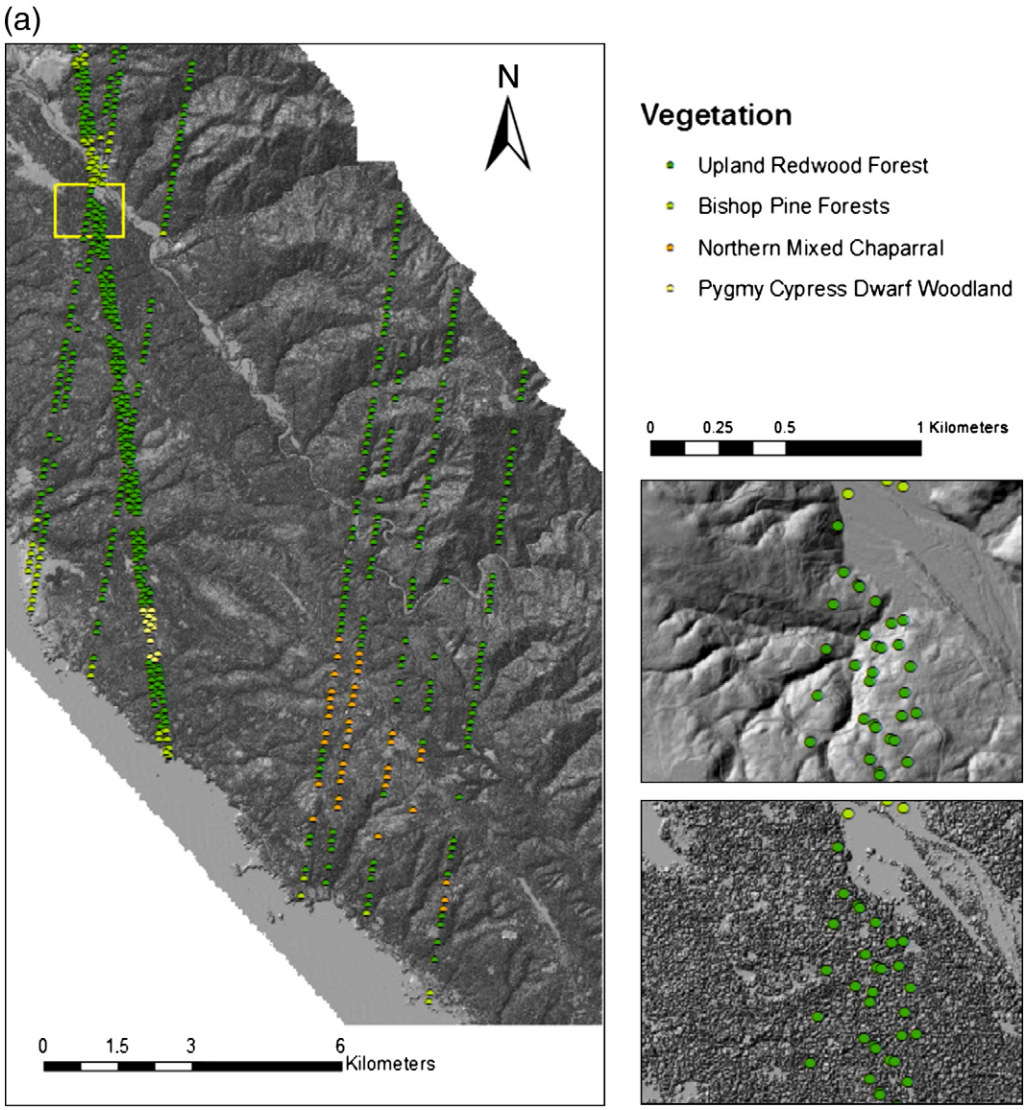

Fig. 3. Topography and vegetation over GLAS shots at the three study sites: a) Mendocino, California, b) Santa Clara, California, and c) Lewis, Washington. On the left of each subfigure is the shaded digital surface model while on the right is the shaded digital elevation model and canopy height model from top to bottom, respectively, for the area indicated by the square on the left image.

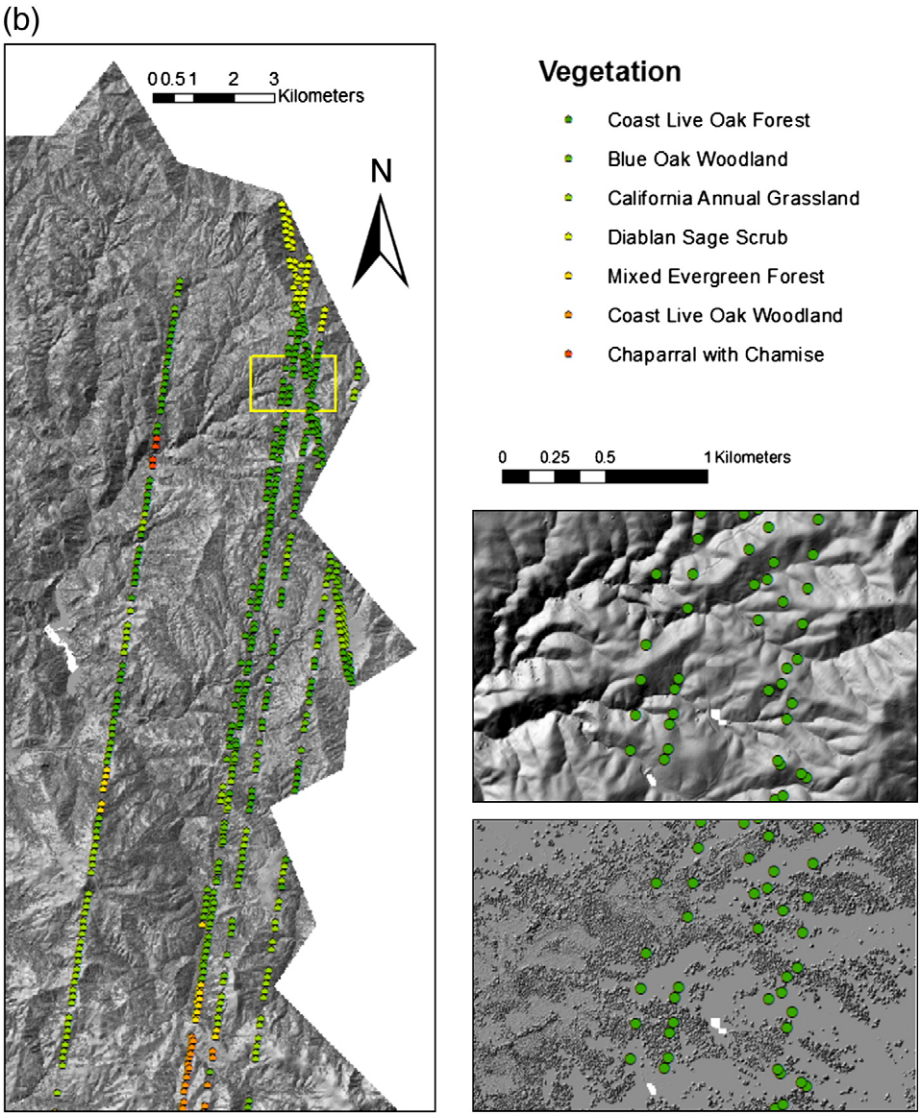

Fig. 3 (*continued*).

south, there are a few patches of forests that have been logged or deforested by Mt. St. Helens explosion but has regrown to lush herbs, shrubs, and young trees. The co-dominant species are Douglas Fir (*Pseudotsuga menziesii*), Western Hemlock (*Tsuga heterophylla*), and Silver Fir (*Abies amabilis*) for conifer forests. A minority of mixed forests (Red Alder *Alnus rubra*, Douglas-fir, and Western Hemlock) also exist in the northern part of the site (Table 1(c)).

The analysis of airborne lidar data indicates that the topography over the GLAS shots for these three sites is generally steep with mean slopes of around 20 degrees (Table 2). The Mendocino and Lewis sites have similar vegetation structure of mean height (~35 m) and canopy cover (~0.9). And they also have some common species such as Douglas Fir. However, the Santa Clara site has much shorter vegetation height (mean height of ~10.7 m) and sparser canopy cover (~0.27) besides its distinct species composition as oak forests/woodlands (Table 1 and 2).

2.2. GLAS data

The NSIDC (National Snow and Ice Data Center) disseminates 15 Level-1 and Level-2 GLAS data products. The products used in this analysis include GLA01 (L1A Global Alimetry) and GLA14 (L2 Land Surface Altimetry) from Release-28. The former stores transmitted and received waveforms from the altimeter while the latter records surface elevations for land and the laser footprint geolocation and reflectance, as well as geodetic, instrument, and atmospheric corrections for range measurements. These two datasets can be linked by the record index.

GLAS waveforms might be contaminated by the atmospheric forward scattering or saturated signals. Therefore, only the cloud-free (the flag FRir_qaFlag = 15 in the GLA14 products) and saturation-free (the saturation index satNdx = 0 in the GLA14 products) shots were analyzed in this study (Chen, 2010; Duncanson et al., 2010); another cloud filter was applied to make sure that the elevation of a waveform must be less than 100 m above the SRTM (Shuttle Radar Topography Mission) elevation; a shot was also excluded if the elevation of its waveform centroid is greater than the maximum elevation or less than the minimum elevation of the coincident airborne lidar points.

Based on the above criteria, a total of 400 (200 in Mendocino, 134 in Santa Clara, and 66 in Lewis) GLAS shots were selected (Table 2). For the California sites, the GLAS shots are from campaign L3B (Feb–Mar, 2005), L3C (May–Jun 2005), L3D (Oct–Nov 2005), L3E (Feb–Mar 2006), L3F (May–Jun 2006), and L3G (Oct–Nov 2006), where L3 stands for Laser 3 and each letter stands for different campaigns of

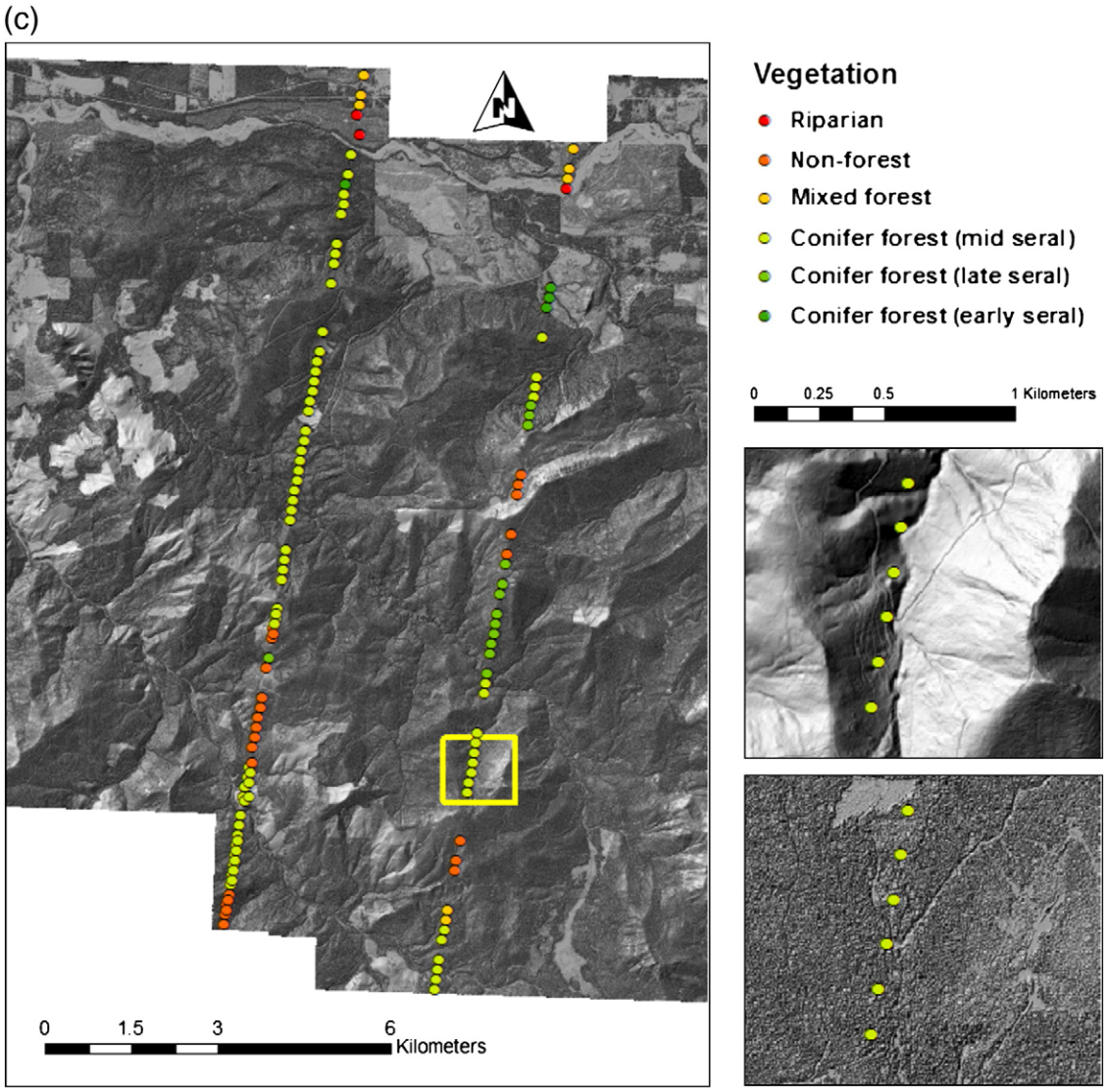

Fig. 3 (*continued*).

data acquisition. For the Lewis site, only shots from L3B, L3D, and L3E are available. The equivalent footprint diameters of these shots vary from 46 to 66 m.

2.3. Airborne lidar data

The airborne lidar data in Mendocino, CA and Lewis, WA were acquired by TerraPoint, LLC in February, 2003 using the Airborne Lidar Terrain Mapping System (ALTMS), a discrete-return, scanning airborne laser altimeter capable of acquiring up to 4 returns per laser pulse (Harding, 2004). The flight altitude varied from 600 m to 2400 m above ground level. The horizontal coordinates are in survey feet referenced to State Plane Coordinate System (NAD 83 HARN) California II and Washington South for the Mendocino and Lewis sites, respectively. Elevations are in international feet referenced to North American vertical Datum 1988 (NAVD88). The orthometric elevations were derived from ellipsoidal elevations using National Geodetic Survey (NGS) GEOID99.

The data in Santa Clara were collected with an Optech ALTM 3100 lidar system by Optimal Geomatics, Inc. from April to May in 2006. The flight altitude varied from 1000 m to 2400 m above ground level. The horizontal coordinates are in State Plane Coordinate System (NAD83) California III in survey feet. The ellipsoid heights were converted to NAVD88 orthometric heights in international feet using NGS GEOID03. The lidar point density of the three study sites is all around 1 laser pulse per square meter. All of these lidar data were obtained through the USGS Center for LIDAR Information Coordination and Knowledge.

3. Methods

3.1. Extracting canopy height using direct methods

The performance of direct methods for maximum canopy height estimation relies on the accurate identification of elevations for both canopy top (z_{ct}) and canopy bottom (z_{cb}) of the tallest plant within a GLAS footprint. Usually, signal start (z_s) and ground peak (z_g) elevation of a waveform are used to approximate canopy top and canopy bottom, respectively (Duong et al., 2008; Neuenschwander et al., 2008; Sun et al., 2008). Therefore, with direct methods,

$$h_g = z_s - z_g \quad (1)$$

where h_g is the maximum canopy height estimated from GLAS data, z_s and z_g are the signal start and ground peak elevation estimated from a GLAS waveform, respectively.

Table 1
Vegetation information for GLAS shots over the three sites: a) Mendocino, California, b) Santa Clara, California, and c) Lewis, Washington. (a) and (b) list the primary vegetation community type and co-dominant species compiled from the California Gap Analysis Project. (c) lists the primary land cover compiled from the Washington Gap Analysis Project. *BVT means broad vegetation type.

(a)

Abb.	Primary community type	Species A	Species B	Species C	Shot count
RF	Upland Redwood Forest	Coast redwood	Douglas fir	Tanoak	111
RF	Upland Redwood Forest	Coast redwood	N/A	N/A	37
RF	Upland Redwood Forest	Coast redwood	Douglas fir	Bishop pine	25
RF	Upland Redwood Forest	Douglas fir	Coast redwood	Oregon oak	6
RF	Upland Redwood Forest	Douglas fir	Coast redwood	N/A	4
PF	Bishop Pine Forests	Non-native annual grassland	Bishop pine	Gowen cypress	10
PF	Bishop Pine Forests	Non-native annual grassland	Bishop pine	Monterey cypress	2
MC	Northern Mixed Chaparral	Eastwood manzanita	Littleberry manzanita	Braken	3
DW	Pygmy Cypress Dwarf Woodland	Eastwood manzanita	Littleberry manzanita	Huckleberry	2

(b)

Abb.	Primary community type	Species A	Species B	Species C	Shot count
CF	Coast Live Oak Forest	Blue oak	Coast live oak	Non-native annual grassland	43
CF	Coast Live Oak Forest	Black oak	Coast live oak	Non-native annual grassland	6
BW	Blue Oak Woodland	Blue oak	Buckeye		10
BW	Blue Oak Woodland	Coast live oak	Valley oak	Blue oak	7
BW	Blue Oak Woodland	Blue oak	Valley oak	Non-native annual grassland	7
BW	Blue Oak Woodland	Blue oak	Valley oak	Buckeye	6
BW	Blue Oak Woodland	Blue oak	Buckeye	Non-native annual grassland	3
BW	Blue Oak Woodland	Blue oak	Non-native annual grassland		2
AG	California Annual Grassland	Non-native annual grassland			27
SS	Diablan Sage Scrub	California sagebrush	Non-native annual grassland		11
EF	Mixed Evergreen Forest	Coast live oak	California bay		6
CW	Coast Live Oak Woodland	Coast live oak	Valley oak	Non-native annual grassland	4
CC	Chaparral with Chamise	Chamise			2

(c)

Abb.	Primary land cover	Shot count
CM	Conifer forest; mid-seral; closed; usually Western Hemlock/Douglas-fir.	32
CM	Conifer forest; mid seral; closed; usually Western Hemlock/Silver Fir, with Douglas-fir at lower elevations.	13
CL	Conifer forest; late seral; closed; usually Silver Fir/Western Hemlock.	5
CE	Conifer forest; early seral; closed; usually Douglas-fir.	3
NF	Non-forested; logged, regrowth to lush herbs, shrubs, and young trees.	7
NF	Non-forested; logged or deforested by Mt. St. Helens explosion; regrowth to lush herbs, shrubs, young trees.	2
MF	Mixed forest; early seral; closed; usually Red Alder/Douglas-fir.	2
RP	Riparian; mixed communities.	2

To identify the signal start, each received waveform is first smoothed using the parameters extracted from its corresponding transmitted waveform, the laser waveform sent from GLAS. Note that each received waveform is a convolution of the transmitted waveform and the illuminated surface reflectance properties so the received waveform is related to transmitted waveform. The transmitted waveform is fitted with a Gaussian function:

$$y = a\exp\left(-\frac{(x-u_t)^2}{2\sigma_t^2}\right) + c \quad (2)$$

where y is the transmitted waveform counts, u_t and σ_t are the mean and standard deviation of the Gaussian function, a and c are constants

Table 2
Topography and vegetation physiognomy for GLAS shots over the three study sites.

Site	Elevation (m) [a]	Slope (deg) [b]	Canopy cover[b]	Maximum canopy ht (m) [a]	Shot count
Mendocino,CA	177.8 (−3.6-622.9)	20.3±9.3	0.90±0.10	35.6±8.4	200
Santa Clara, CA	406.2 (207.1-575.2)	20.6±8.4	0.27±0.22	10.7±6.0	134
Lewis, WA	794.2 (454.1-1182.2)	21.3±9.2	0.90±0.11	35.0±10.7	66

[a] The first number is the mean, the numbers in the parentheses are the minimum and maximum values.
[b] The first number is the mean and the second is the standard deviation. The terrain and canopy characteristics are derived from airborne lidar data.

(Fig. 4(a)). Then, the received GLAS waveform is smoothed with a Gaussian filter of $2\sigma_t$ and a window size of $6\sigma_t$ to avoid the background noise to be detected as signal (Sun et al., 2008) (Fig. 4(b)). The signal start is identified as the first bin location where the waveform intensity is a certain threshold above the mean background noise μ_b in the waveform. Previous studies have used different thresholds, including $3\sigma_b$ (Sun et al., 2008), $4\sigma_b$ (Lefsky et al., 2005), or $4.5\sigma_b$ (Lefsky et al., 2007), where σ_b is the standard deviation of the background noise. Both μ_b and σ_b are recorded in the GLA01 product. This study will examine a sequence of thresholds $n\times\sigma_b$ ($n=0.5,1,\ldots,5$) and see which threshold produces the best match with the highest Z coordinate(s) for the corresponding airborne lidar point cloud within each GLAS footprint.

The ground peak identification is usually based on the Gaussian decomposition results. The GLA14 products record the parameters (mean, standard deviation, and amplitude) for up to 6 decomposed Gaussian peaks. However, there is no widely accepted method for estimating ground elevation from Gaussian peaks (Duong et al., 2008, Rosette et al., 2008, Sun et al., 2008, Chen, 2010). In this study, two sets of metrics derived from Gaussian decomposition are used to evaluate the ground elevation: 1) the elevation of individual Gaussian peak (z_i, $i=1,\ldots,6$), and 2) the elevation of the peak of maximum amplitude among the lowest n peaks ($z_{\max,n}$, $n=2,\ldots,6$). Assuming the amplitude of each Gaussian peak is a_i ($i=1,2,\ldots,6$),

$$z_{\max,n} = z_{a_i=\max(a_1,a_2,\ldots,a_n)},\ \text{where } i = 1,\ldots,n \text{ and } n = 2,\ldots,6 \quad (3)$$

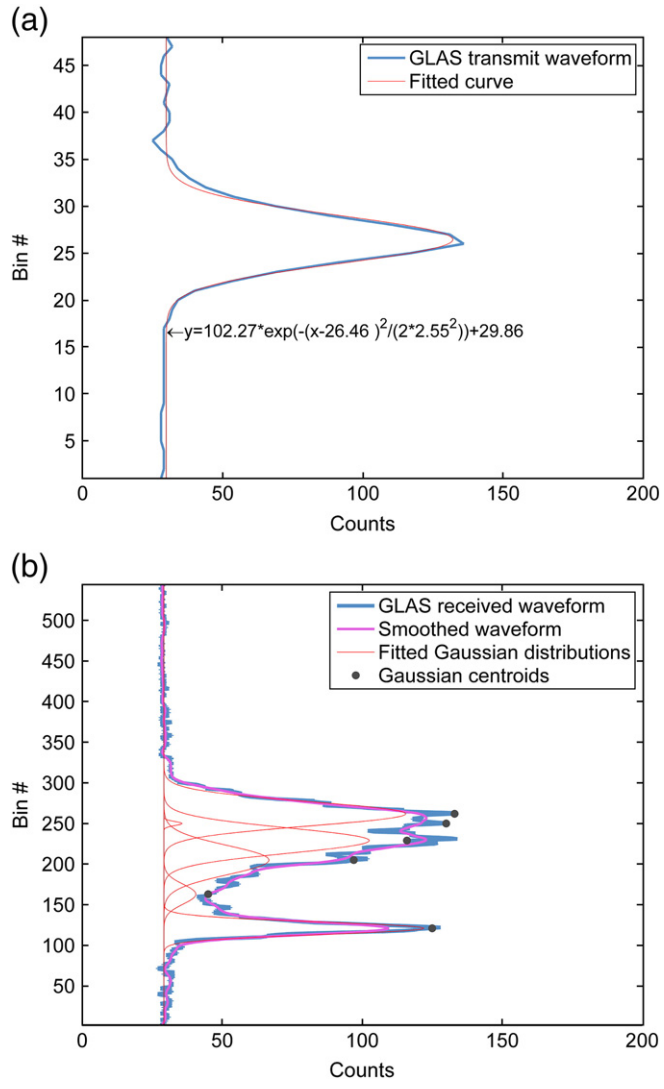

Fig. 4. Examples of (a) a transmitted waveform, and (b) a received GLAS waveform. The smoothed waveform and fitted Gaussian distribution are also shown in (b).

3.2. Modeling canopy height using statistical methods

A total of three models are developed to predict maximum canopy height as follows:

$$h_g = a_1 \times \text{wfExt} - a_2 \times \text{demExt} \quad (4)$$

$$h_g = a_1 \times \text{wfExt} - a_2 \times (\text{leadExt} + \text{trailExt}) \quad (5)$$

$$h_g = a_1 \times \text{wfExt} - (a_2 \times (\text{leadExt} + \text{trailExt}))^{a3} \quad (6)$$

where h_g is the predicted maximum canopy height from GLAS waveform metrics; wfExt, leadExt, and trailExt are the GLAS waveform extent, leading-edge extent, and trailing-edge extent, respectively. Leading-edge extent is the vertical elevation difference between signal start and the highest bin that is at half maximum intensity; trailing-edge extent is the vertical elevation difference between signal end and the lowest bin that is at half maximum intensity (Lefsky et al., 2007). demExt is the DEM extent, which is the difference between maximum and minimum elevation of airborne lidar DEM within each GLAS footprint.

Only a few studies (Lefsky et al., 2005; Rosette et al., 2008) have developed statistical models to predict maximum canopy height from GLAS. The statistical models in these studies included waveform extent as an independent variable. To remove the broadening effects caused by the sloped terrain, DEM-based terrain metrics that quantify the vertical elevation range within or surrounding footprints were included in the models of these studies. For example, Lefsky et al. (2005) used the elevation range within three neighborhood windows (3×3, 5×5, 7×7) of 30 m- or 90 m-SRTM DEM around each GLAS shot. Rosette et al. (2008) used the elevation range within a 7×7 neighborhood of 10 m-DEM. Considering that conventional DEMs might not adequately characterize topography over forest areas, Lefsky et al. (2007) and Pang et al. (2008) estimated canopy height with metrics derived from waveform themselves. Lefsky et al. (2007) proposed multiple transformations of three waveform metrics (waveform extent, leading-edge extent, and trailing-edge extent) and then used stepwise regression to develop correction factors for broadened waveform extent to estimate mean canopy height. A later study by Pang et al. (2008) found that such an approach led to many unrealistic estimates of canopy height and thus proposed a simpler nonlinear model like Model (6) to estimate the crown-area weighted mean canopy height. In light of these studies, the development of statistical models for estimating maximum canopy height is based on several criteria: 1) to avoid "over-fitting", the model should be simple according to *Occam's razor* or the law of parsimony that the simplest explanation or strategy tends to be the best one, 2) instead of relying on ancillary DEMs, the model will be based on metrics derived from waveforms themselves. Models (5) and (6) are developed based on these criteria. Note that Model (6) has been used in Pang et al. (2008) to estimate crown-area weighted mean canopy height instead of maximum canopy height. Model (5) is developed in this study to examine how an even simpler linear model performs when compared to the nonlinear Model (6). Model (4) is supposed to generate the best results since it is based on airborne lidar data. Therefore, this model is mainly used as a benchmark to examine how the models based on waveform metrics themselves perform compared to the models based on high-quality DEMs. Models (4)–(6) are referred as DEM linear model, edge-extent linear model, and edge-extent nonlinear model hereinafter. To calculate the maximum canopy height from airborne lidar data for developing these statistical models, the Z coordinates of all lidar points within a GLAS footprint are subtracted by the elevations of the corresponding DEM cells to remove the terrain variations.

The calculation of waveform, leading-edge, and trailing-edge extents requires the elevations of waveform signal start and end. The elevation of signal end is identified using an approach similar to the one finding the signal start in the direct methods, which is to examine a sequence of thresholds $n\times\sigma_b$ ($n=0.5,1,\ldots,5$) and see which threshold produces the best match with the lowest Z coordinates for the corresponding airborne lidar point cloud within each GLAS footprint.

The coefficient of determination (R^2) is perhaps the single most extensively used measure of goodness of fit for regression models (Kvålseth, 1985). However, there are problems with R^2 for the no-intercept model (Anderson-Sprecher, 1994). Using five-fold cross-validation, this study assesses different methods at individual sites based on a number of statistics including the difference (ε_cv), adjusted R-square (R^2_a_cv), root mean square error (RMSE_cv), and Akaike information criterion with second-order bias correction (AIC_cv) between the canopy height predicted from GLAS data (h_g) and the canopy height derived from airborne lidar data (h_a) (Chen et al., 2007a).

3.3. Examining generalizability of the statistical models

GLAS is a large-footprint satellite lidar system that aims to map canopy height at the regional and global scales. Therefore, it is critical to evaluate the generalizability of the developed statistical models. This study will test model generalizability at inter-site and intra-site

levels: the inter-site generalizability means that how a model developed at one site performs at other sites; the intra-site generalizability refers to that how a model developed for one vegetation community type within a site can be applied to other community types within the same site (Table 1). To extrapolate the statistical models to a larger area, the models developed at the inter- and intra-site levels require different amount of ground-truth data for model calibration and maps of different details for stratification of the whole study area. Therefore, the model generalizability test at these two levels can help determine how to optimally stratify a study area so that both the efforts of ground-truthing and the model prediction errors can be minimized.

A combination of exploratory data analysis and advanced statistical analysis are used to examine the model generalizability. The exploratory data analysis involves the evaluation of model fitting statistics when a model developed at any particular site is applied at the other two. The evaluated statistics include difference (ε), correlation (r), root mean square error (RMSE), and Akaike information criterion with second-order bias correction (AIC) between the canopy height predicted from GLAS data (h_g) and the canopy height derived from airborne lidar data (h_a). Note that correlation (r) instead of adjusted R-square is used because adjusted R-square is not appropriate if h_g is highly biased compared to h_a. Due to the limitation of space, only the results of the exploratory data analysis at the inter-site level are reported in this study.

The advanced statistical analysis deals with the use of mixed-effects model to examine whether there are random effects in the model coefficients, which is conducted at both inter-site and intra-site levels. Eqs. (4)–(6) are called fixed-effects models since the model coefficients are constants. Mixed-effects models can be developed corresponding to Eqs. (4)–6). Taking Eq. (5) as an example, the corresponding general mixed-effect model could be as follows:

$$h_{g,ij} = \beta_{1,i} \times \mathrm{wfExt}_{ij} - \beta_{2,i} \times \left(\mathrm{leadExt}_{ij} + \mathrm{trailExt}_{ij}\right) + \varepsilon_{ij} \quad (7)$$

$$\beta_{1,i} = \beta_1 + u_{1,i} \quad (8)$$

$$\beta_{2,i} = \beta_2 + u_{2,i} \quad (9)$$

where i represents individual sites (when the model is developed at the inter-site level) or primary vegetation community types within each site (when the model is developed at the intra-site level), j refers to individual GLAS shots in site i or vegetation community type i, and ε_{ij} is the residuals.

Combine Eqs. (7)–(9), and we have:

$$\begin{aligned} h_{g,ij} = {} & \beta_1 \times \mathrm{wfExt}_{ij} - \beta_2 \times \left(\mathrm{leadExt}_{ij} + \mathrm{trailExt}_{ij}\right) + u_{1,i} \\ & \times \mathrm{wfExt}_{ij} - u_{2,i} \times \left(\mathrm{leadExt}_{ij} + \mathrm{trailExt}_{ij}\right) + \varepsilon_{ij} \end{aligned} \quad (10)$$

where β_1 and β_2 are fixed-effects, while $u_{1,i}$, $u_{2,i}$, and ε_{ij} are random effects. If any of the random effects $u_{1,i}$ and $u_{2,i}$ is statistically significant, it implies that the corresponding fixed-effects model does not have good generalizability across different sites or across different vegetation community types within a site.

3.4. Simulation of the footprint size effects on canopy height estimation

Extracting canopy height from GLAS data is mainly complicated by the uncertainty of finding the exact vertical elevations of canopy top and bottom from GLAS waveforms at the tree level. Given its large footprint, it is difficult for GLAS to characterize canopy structure at the individual tree level because GLAS waveforms are a mixture of signals from all trees and terrain within the footprint. To reduce the uncertainty in canopy height estimation, the most effective approach might be reducing the waveform footprint size. However, little research has been done to investigate the effects of footprint size on canopy height estimation, although it has important implications for determining the optimal footprint size for next-generation satellite lidar systems.

A proof-of-concept approach as follows is used to simulate the effects of footprint size on canopy height estimation. First, airborne lidar point clouds are extracted around the centers of the GLAS footprints. The elevation difference between the highest and lowest point within a footprint is considered as a surrogate of GLAS waveform extent (wfExt). The DEM extent (demExt) is extracted from the DEM generated from airborne lidar data. The ground peak elevation z_g is the weighted mean elevation of DEM while z_s is the elevation of the highest point. To calculate the maximum canopy height h_a, the Z coordinates of raw lidar points are normalized by subtracting the corresponding ground elevation. The direct method and the DEM linear model are tested at four footprint sizes varying from 40 m to 10 m by every 10 m.

3.5. Registering airborne lidar data and GLAS data

The airborne lidar and GLAS data have to be georeferenced to the same horizontal and vertical datums for comparison purpose. The geodetic latitude, longitude, and elevation of GLAS data are referred to the TOPEX/Poseidon ellipsoid, which was converted into WGS 84 datum. The airborne lidar data have orthometric elevations in NAVD 88 datum, which were converted to ellipsoid heights in NAD 83 datum using the GEOID99 or GEOID03 model of National Geodetic Survey (NGS). WGS 84 datum is earth-centered while NAD 83 datum is not even though they use almost the same ellipsoid, so the datum of airborne lidar data is further converted to WGS84, which is accomplished using the NGS HTDP (Horizontal Time Dependent Positioning) software (Chen, 2010).

To derive ground elevation from airborne lidar data, the ground returns are first extracted from the raw point clouds and then interpolated into DEMs of 1×1 m cells using the Tiffs (Toolbox for Lidar Data Filtering and Forest Studies) software (Chen, 2007; Chen et al., 2007b; Chen, 2009). Considering the spatial distribution of transmit pulse intensity within a footprint, the elevation of cells within a footprint is weighted using the following equation:

$$\begin{aligned} w &= e^{\left(-2\sqrt{(x'/a)^2 + (y'/b)^2}\right)} \\ x' &= (x - x_0)\sin\alpha + (y - y_0)\cos\alpha \\ y' &= (y - y_0)\sin\alpha - (x - x_0)\cos\alpha \end{aligned} \quad (11)$$

where w is the weight for any airborne lidar DEM grid cell within a footprint; a and b are the semi-major and semi-minor axes of the footprint; (x,y) and (x_0,y_0) are the coordinates for the cell and the footprint center, respectively; x' and y' are coordinates of the cell along major and minor axes, respectively, with the footprint center as the origin of the coordinate system; α is the azimuth angle of the major-axis of the footprint. The weights in Eq. (11) are normalized so that their sum is 1 before averaging. The weighted mean elevation z_w from airborne lidar DEM is used to identify the Gaussian peak that mostly matches the ground.

The GLAS shots over open and flat terrain, called calibration shots, are analyzed to check whether there is systematic difference between airborne lidar and GLAS data (Chen, 2010). The waveforms of these shots should have only one distinct peak indicating the mean ground elevation. Two metrics are derived from airborne lidar data within each GLAS footprint to help identify the GLAS shots over open and flat terrain: 1) the ratio n_r between the number of non-terrain returns and all returns, which indicates openness of the footprint area, 2) the mean slope s_w weighted using Eq. (11). If n_r is less than 5% and s_w is less than 5°, a shot is considered as a calibration shot.

Table 3
Difference between various ground elevation metrics derived from GLAS z_g and the weighted mean ground elevation z_w derived from airborne lidar data within footprints. A total of 11 ground elevation metrics z_g are assessed, including the elevation of 6 Gaussian peaks (z_i, $i=1, \ldots, 6$) and 5 maximum peak ($z_{max,n}$, $n=2, \ldots, 6$). $z_{max,n}$ means the elevation of the peak of the maximum amplitude among the lowest n peaks.

Peak	$z_g - z_w$ (m)		
	Mendocino	Santa Clara	Lewis
z_1	-4.3 ± 5.6	-7.3 ± 5.6	-4.6 ± 6.2
z_2	4.7 ± 7.4	-3.0 ± 4.8	5.3 ± 7.4
z_3	9.8 ± 7.8	0.4 ± 4.1	11.8 ± 7.9
z_4	14.2 ± 7.6	3.8 ± 4.2	16.5 ± 7.4
z_5	18.2 ± 7.7	7.3 ± 4.9	21.1 ± 7.3
z_6	23.0 ± 8.0	11.6 ± 5.7	25.7 ± 8.6
$z_{max,2}$	3.2 ± 7.7	-4.4 ± 5.5	3.7 ± 8.1
$z_{max,3}$	5.9 ± 7.7	-2.0 ± 4.2	7.8 ± 8.5
$z_{max,4}$	7.3 ± 8.3	-0.9 ± 4.1	8.9 ± 9.2
$z_{max,5}$	9.3 ± 9.6	0.0 ± 4.0	10.3 ± 9.4
$z_{max,6}$	13.5 ± 10.3	1.0 ± 4.7	15.6 ± 11.9

Table 4
Difference 1) between signal start (z_s) and the highest elevation (z_{max}), and 2) between signal end (z_e) and the lowest elevation (z_{min}) when different thresholds ($n \times \sigma_b$, where σ_b is the standard deviation of the waveform background signal) are used for the three study sites.

n	Mendocino		Santa Clara		Lewis	
	$z_s - z_{max}$ (m)	$z_e - z_{min}$ (m)	$z_s - z_{max}$ (m)	$z_e - z_{min}$ (m)	$z_s - z_{max}$ (m)	$z_e - z_{min}$ (m)
0.5	5.7 ± 6.2	-9.8 ± 5.5	8.0 ± 6.5	-6.5 ± 4.4	9.5 ± 9.1	-9.0 ± 6.8
1	3.7 ± 5.3	-6.6 ± 5.0	5.5 ± 5.3	-5.3 ± 4.2	6.5 ± 8.0	-6.5 ± 5.9
1.5	2.1 ± 4.5	-4.5 ± 4.8	3.7 ± 4.7	-4.3 ± 3.6	3.9 ± 5.8	-4.5 ± 5.8
2	1.0 ± 4.2	-3.1 ± 4.5	2.5 ± 4.3	-3.4 ± 3.7	2.5 ± 5.2	-2.8 ± 5.4
2.5	0.1 ± 4.0	-1.6 ± 4.5	1.5 ± 4.1	-2.5 ± 3.4	1.4 ± 4.7	-1.7 ± 5.5
3	-0.6 ± 3.8	-0.4 ± 4.5	0.5 ± 4.0	-1.8 ± 3.2	0.1 ± 5.5	-0.9 ± 5.5
3.5	-1.2 ± 3.8	0.6 ± 4.7	-0.1 ± 3.9	-1.2 ± 3.0	-0.6 ± 5.5	0.4 ± 5.8
4	-1.8 ± 3.9	1.4 ± 5.0	-0.7 ± 3.8	-0.7 ± 3.0	-1.1 ± 5.5	1.9 ± 6.8
4.5	-2.3 ± 3.8	2.1 ± 5.2	-1.1 ± 3.8	-0.3 ± 3.0	-1.6 ± 5.4	2.6 ± 6.8
5	-2.7 ± 3.8	2.7 ± 5.3	-1.4 ± 3.7	0.1 ± 2.9	-2.0 ± 5.4	3.3 ± 6.8

4. Results and discussion

4.1. Systematic difference between GLAS and airborne lidar data

Thirteen of the 134 shots in the Santa Clara site were identified as calibration shots. The elevation difference between the distinct GLAS peak and weighted mean ground elevation z_w from airborne lidar is 0.05 ± 0.49 m for these shots. Due to the closed canopy in the Mendocino and Lewis sites, no shots can be counted as calibration shots. However, in the coastal area of the Mendocino site, there are a large number of shots located on the beach (not shown in Fig. 3(b)) and 50 of them were identified as calibration shots. The elevation difference is 0.05 ± 0.54 m for these 50 shots. These small values indicate that the systematic differences between GLAS and airborne lidar data are relatively small. Although there are no calibration shots for the Lewis site, the difference is expected to be small given that the same airborne lidar system as the one at the Mendocino site was used.

Table 5
Performance of direct methods for estimating maximum canopy height. ε, r, and RMSE are the difference, correlation, and root mean square error between estimated canopy height and the canopy height from airborne lidar data, respectively.

Site	ε (m)	r	RMSE (m)
Mendocino	−1.99	0.47	9.12
Santa Clara	3.69	0.58	7.24
Lewis	0.18	0.62	10.25

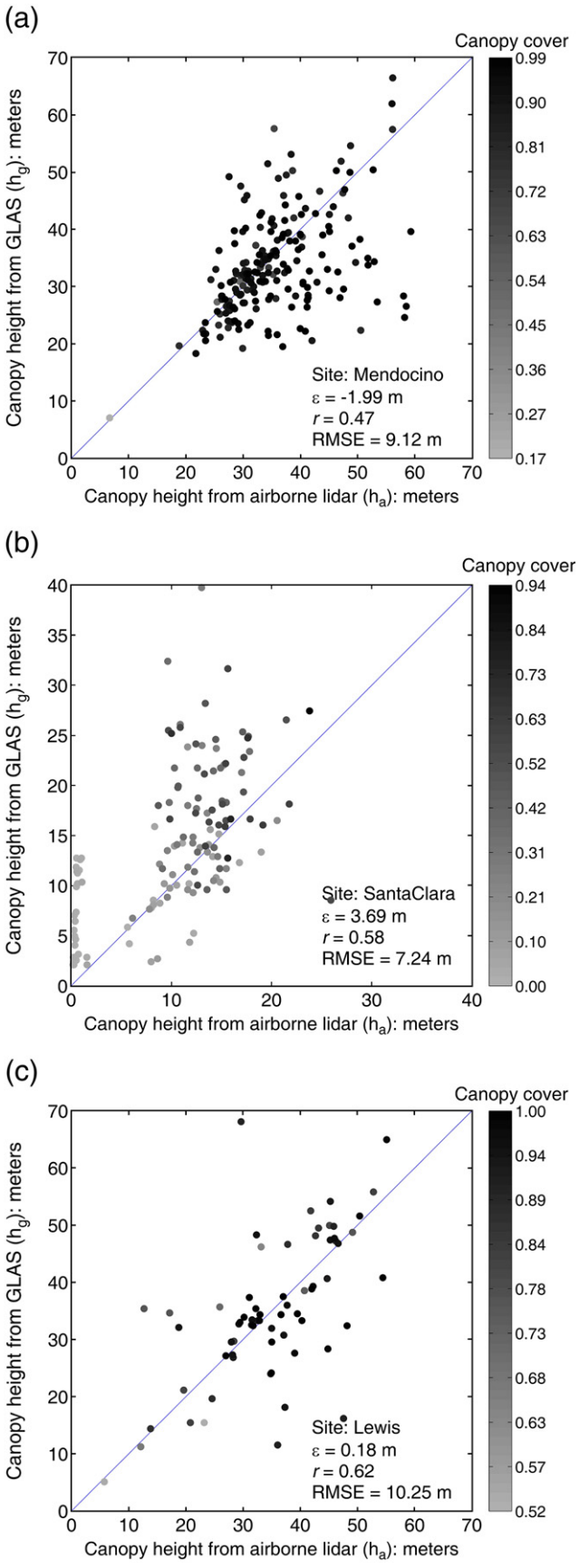

Fig. 5. Comparison between canopy height extracted from GLAS (h_g) using direct methods and the corresponding canopy height derived from airborne lidar data (h_a) for the (a) Mendocino, (b) Santa Clara, and (c) Lewis sites. ε, r, and RMSE are the difference, correlation, and root mean square error between h_g and h_a, respectively.

Table 6
Three regression models (DL: DEM linear model; EN: Edge-extent linear model; and EN: Edge-extent nonlinear model) developed at the Mendocino, Santa Clara, and Lewis sites, respectively. ε_cv, R^2_a_cv, RMSE_cv, and AIC_cv are the difference, adjusted R-square, root mean square error, Akaike information criterion with second-order bias correction calculated with five-fold cross-validation. $\Delta = \text{AIC\_cv} - \text{AIC}_{\min}$, where $\text{AIC}_{\min}$ is the minimum of the different AIC_cv values at a site.

Site	Model type	ε_cv	R^2_a_cv	RMSE_cv	AIC_cv	Δ	Model
Mendocino	DL: DEM linear	−0.30	0.46	6.18	731.90	0.00	M_DL: $h = 0.87 \times \text{wfExt} - 0.29 \times \text{demExt}$
	EL: Edge-extent linear	−0.38	0.42	6.40	750.51	18.61	M_EL: $h = 0.85 \times \text{wfExt} - 0.17 \times (\text{leadExt} + \text{trailExt})$
	EN: Edge-extent nonlinear	−0.24	0.38	6.37	748.55	16.65	M_EN: $h = 0.85 \times \text{wfExt} - (0.08 \times (\text{leadExt} + \text{trailExt}))^{1.82}$
Santa Clara	DL: DEM linear	−0.39	0.34	4.88	427.32	0.00	S_DL: $h = 0.64 \times \text{wfExt} - 0.27 \times \text{demExt}$
	EL: Edge-extent linear	−0.40	0.28	5.08	438.18	10.87	S_EL: $h = 0.43 \times \text{wfExt} - 0.02 \times (\text{leadExt} + \text{trailExt})$
	EN: Edge-extent nonlinear	−0.06	0.31	4.97	436.31	9.00	S_EN: $h = 0.46 \times \text{wfExt} - (0.05 \times (\text{leadExt} + \text{trailExt}))^{4.45}$
Lewis	DL: DEM linear	−1.13	0.24	9.31	301.70	0.00	L_DL: $h = 0.84 \times \text{wfExt} - 0.31 \times \text{demExt}$
	EL: Edge-extent linear	−1.18	0.21	9.47	302.73	1.03	L_EL: $h = 0.81 \times \text{wfExt} - 0.17 \times (\text{leadExt} + \text{trailExt})$
	EN: Edge-extent nonlinear	−0.88	0.21	9.26	301.87	0.16	L_EN: $h = 0.80 \times \text{wfExt} - (0.08 \times (\text{leadExt} + \text{trailExt}))^{1.54}$

4.2. Airborne lidar data filtering and DEM generation

The canopy height and terrain elevation derived from airborne lidar are affected by the filtering of the lidar point cloud, the process of identifying ground returns. Unlike many other software packages that require manual editing of the point cloud, Tiffs uses an automatic filtering algorithm (Chen et al., 2007b; Chen, 2009) to search ground returns and generate a DEM. The filtering algorithm achieved the best overall performance when compared with other eight algorithms that were tested with the ISPRS Commission III/WG3 benchmark dataset including sites ranging from urban to rural areas with different complexity (Chen et al., 2007b). Although there is no direct ground truth data to validate the filtering accuracy, a DEM generated by automatic classification followed by manual inspection is available through the Planetary Geodynamics Laboratory at NASA's Goddard Space Flight Center for the Mendocino site (Harding, 2004). It was found that the difference of weighted mean ground elevation between the Tiffs DEM and NASA DEM is 0.01 ± 0.73 m at the 200 GLAS shot locations. The small mean difference indicates that the automatic approach used in Tiffs achieved comparable accuracy with the manually edited DEM. There are no DEMs available for the other two sites, but it is reasonable to assume that the DEMs at these two sites are comparable, or with even better quality, given that terrain and vegetation are similar to those at the Lewis site and less complex than those at the Santa Clara site.

4.3. Correspondence between Gaussian peak elevation metrics and ground elevation

As mentioned earlier in Section 3.1, two set of metrics derived from Gaussian decomposition are used to evaluate the ground elevation: 1) the elevation of individual Gaussian peak (z_i, $i = 1, \ldots, 6$), and 2) the elevation of the peak of maximum amplitude among the lowest n peaks ($z_{\max,n}$, $n = 2, \ldots, 6$).

Among the first set of elevation metrics, the lowest peak (z_1) significantly underestimates the ground elevation at these three study site. The average biases are -4.3 ± 5.6 m, -7.3 ± 5.6 m, and -4.6 ± 6.2 m for the Mendocino, Santa Clara, and Lewis sites, respectively (Table 3). At the Mendocino and Lewis sites, all Gaussian peaks except the lowest one overestimate the ground elevation on average. At the Santa Clara site, the third lowest peak (z_3) is the closest to the ground elevation on average.

Among the second set of elevation metrics, it was found that the stronger peak among the last two ($z_{\max,2}$) is closer to the ground elevation than any other peaks of maximum amplitude at the Mendocino and Lewis sites. This is consistent with the results from another study of 482 GLAS shots over the Appalachians Mountain in North Carolina, where $z_{\max,2}$ matches the ground elevation well (with a bias of 0.38 ± 7.02 m) (Chen, 2010). However, on average $z_{\max,2}$ overestimates the ground elevation by a larger magnitude of 3.2 ± 7.7 m and 3.7 ± 8.1 m for the Mendocino and Lewis sites, respectively. This might be because there is not enough energy returned from the terrain due to the high biomass and closed canopy above ground at these two sites. At the Santa Clara site, the strongest peak among the lowest five Gaussian peaks has the smallest bias (0.0 ± 4.0 m) when compared to the ground elevation. Compared to the conifer sites, the canopy at this site is open and sparse. If trees are concentrated at the lower side the slope in a footprint, it is possible that the ground peak is higher than most of the other Gaussian peaks, which explains why it is not the lowest peaks that correspond to the ground elevation. This indicates that, if direct methods are used for estimating canopy maximum height, the ground elevation peaks over woodlands may need to be extracted separately from those over other land covers.

4.4. Optimal thresholds for signal start and end of GLAS waveforms

Table 4 lists the elevation difference between the GLAS waveform signal start (z_s) and the highest elevation ($z_{\max}$) derived from airborne

Table 7
Inter-site analysis of the three regression models (DL: DEM linear model; EN: Edge-extent linear model; and EN: Edge-extent nonlinear model) for predicting canopy height. ε, r, RMSE, and AIC are the difference, correlation, root mean square error, and Akaike information criterion with second-order bias correction, respectively. $\Delta = \text{AIC} - \text{AIC}_{\min}$, where $\text{AIC}_{\min}$ is the minimum of the different AIC values at a site.

Model	Mendocino site					Santa Clara site					Lewis site				
	ε (m)	r	RMSE(m)	AIC	Δ	ε (m)	r	RMSE (m)	AIC	Δ	ε (m)	r	RMSE(m)	AIC	Δ
M_DL	−0.30	0.71	6.07	727.5	0.0	4.88	0.62	7.45	540.3	118.4	0.75	0.64	9.20	299.3	3.1
M_EL	−0.39	0.69	6.34	744.8	17.3	7.67	0.58	10.10	621.2	199.3	0.72	0.61	9.35	301.5	5.2
M_EN	−0.22	0.68	6.27	740.2	12.7	8.63	0.58	10.86	640.5	218.6	0.68	0.60	9.24	299.9	3.6
S_DL	−10.59	0.71	12.15	1005.0	277.6	−0.38	0.62	4.77	421.9	0.0	−9.79	0.64	12.76	344.7	48.5
S_EL	−15.95	0.69	17.14	1142.8	415.3	−0.38	0.58	5.00	434.1	12.2	−15.16	0.61	17.34	385.3	89.0
S_EN	−24.68	−0.28	31.06	1380.5	653.0	−0.10	0.59	4.87	427.4	5.4	−23.37	−0.14	30.02	457.7	161.4
L_DL	−1.92	0.71	6.30	744.2	16.8	3.77	0.62	6.57	509.1	87.2	−1.13	0.64	8.99	296.3	0.0
L_EL	−2.31	0.69	6.64	765.3	37.9	6.70	0.58	9.20	598.6	176.7	−1.07	0.61	9.16	298.8	2.5
L_EN	−1.69	0.69	6.42	751.8	24.3	7.52	0.58	9.86	617.0	195.0	−0.73	0.61	9.08	297.6	1.3

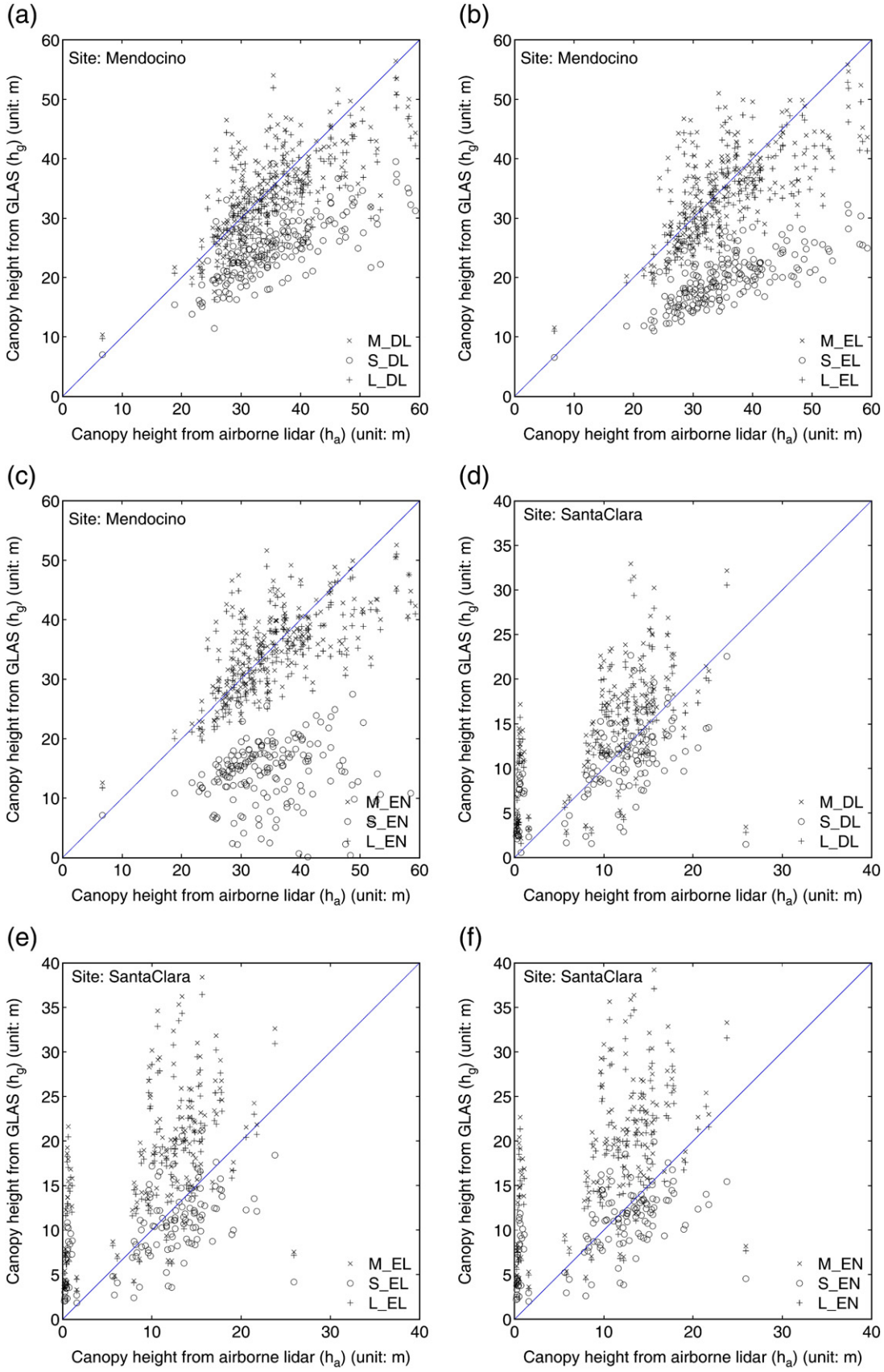

Fig. 6. Inter-site analysis of the regression models for predicted canopy height from GLAS (h_g). Each subfigure shows not only the predicted canopy height using the model developed at a particular site, but also the predicted canopy heights using the two other models developed at the other two sites. Subfigures (a)-(c), (d)-(f), (g)-(i) are the model test results for Mendocino, Santa Clara, and Lewis, respectively. Subfigures (a), (d), and (g) are for the DEM linear models (DL); subfigures (b), (e), and (h) are for the edge-extent linear model (EL); subfigures (c), (f), and i) are for the edge-extent nonlinear models (EN). Refer to Table 6 for the specific models.

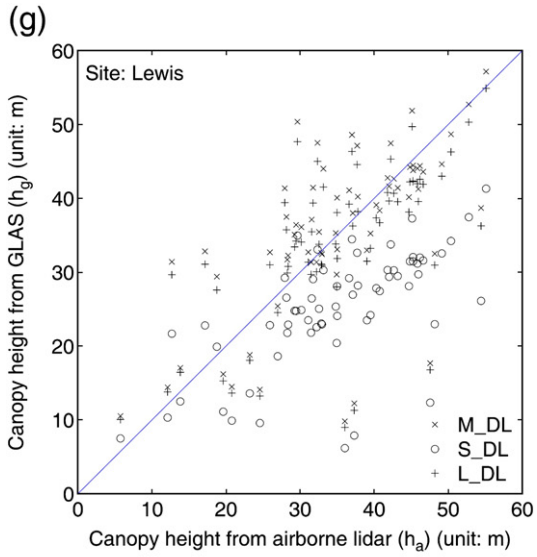

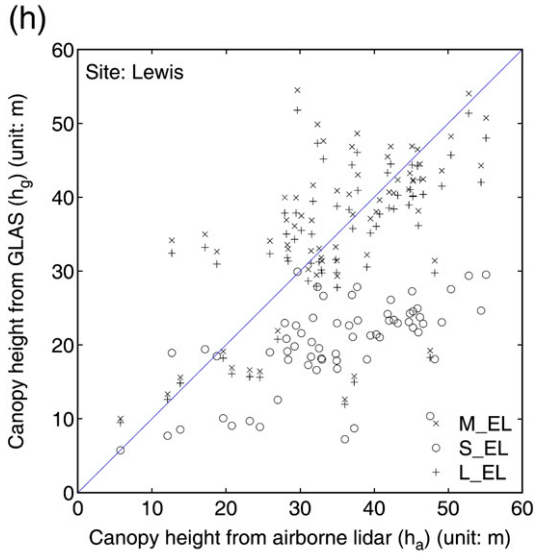

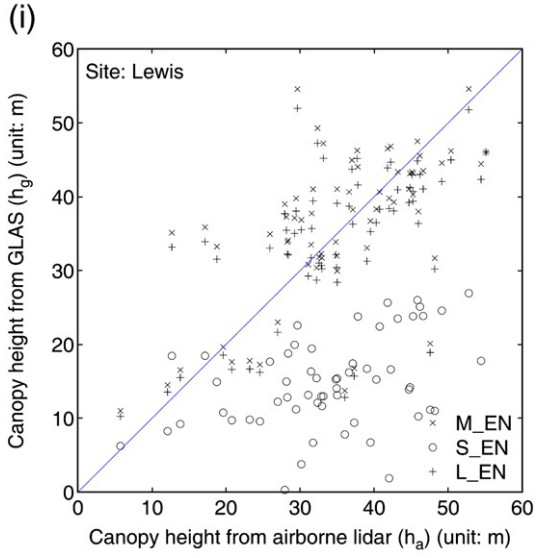

Fig. 6 (*continued*).

lidar data as well as the difference between the GLAS waveform signal end (z_e) and the lowest elevation (z_{min}) from airborne lidar when different thresholds ($n \times \sigma_b$) are used. The threshold that matches the airborne lidar data is considered as the optimal threshold. There are no consistent optimal thresholds that can be applied over all three sites. For the Mendocino site, the optimal threshold for signal start and end are $2.5\sigma_b$ and $3\sigma_b$, respectively. For the Lewis site, the optimal threshold for signal start and end are $3\sigma_b$ and $3.5\sigma_b$, respectively. The Santa Clara site has the largest optimal thresholds $3.5\sigma_b$ and $5\sigma_b$ to match z_{max} and z_{min}, respectively. The preliminary analysis (results not shown) indicates that it was the background noise and relatively weak signals from the canopy top and lowest elevation that made it difficult to identify the signal start and end in a consistent way. To develop a method that can consistently detect the signal start and end, we may need airborne lidar data with higher point density since the current lidar data might miss some treetops of the conifer trees.

4.5. Comparison of different methods

4.5.1. Direct methods

Fig. 6(a)–(c) show the canopy height extracted from GLAS data using direct methods (h_g) versus the maximum canopy height (h_a) derived from airborne lidar data. Note that h_a is determined by the elevation difference of the canopy top (z_{ct}) and canopy bottom (z_{cb}) of the tallest plant within a footprint. The difference $\varepsilon \pm$ RMSE between h_g and h_a are -1.99 ± 9.12 m, 3.69 ± 7.24 m, and 0.18 ± 10.25 m for the Mendocino, Santa Clara, and Lewis sites, respectively. The correlation r between h_g and h_a is the highest at Lewis site (0.62), followed by the Santa Clara site (0.58) and the Mendocino site (0.47) (Table 5).

It is suspected that several factors can lead to the discrepancy between h_g and h_a: i) the elevation of the highest element within a footprint (z_{max}) is not necessarily at the top of the tallest plant (z_{ct}). For example, the highest point might be the top of a shorter tree that is located in higher elevation (Fig. 1(d). It might also simply be the terrain instead of any vegetation (see Fig. 1(e)), which could occur for sparse canopy over steep terrain such as the Santa Clara woodland site; ii) the tallest tree is not located in the ground peak elevation so that z_{cb} is not the same as the GLAS-derived ground peak z_g (see Fig. 1 (b)–(e)); and iii) there exists a difference between the elevation of the detected signal start (z_s) and z_{max}. Overall, the error budget of GLAS canopy height compared to canopy height derived from airborne lidar can be summarized as:

$$\varepsilon = h_g - h_a = \varepsilon_{z_s,z_{max}} + \varepsilon_{z_{max},z_{ct}} + \varepsilon_{z_{cb},z_w} + \varepsilon_{z_w,z_g} \quad (12)$$

where $\varepsilon_{z_s,z_{max}} = z_s - z_{max}$, $\varepsilon_{z_{max},z_{ct}} = z_{max} - z_{ct}$, $\varepsilon_{z_{cb},z_w} = z_{cb} - z_w$, and $\varepsilon_{z_w,zg} = z_w - z_g$, and the corresponding mean error is:

$$E(\varepsilon) = E(\varepsilon_{z_s,z_{max}}) + E(\varepsilon_{z_{max},z_{ct}}) + E(\varepsilon_{z_{cb},z_w}) + E(\varepsilon_{z_w,z_g}) \quad (13)$$

Basically, ε_{z_{cb},z_w} is affected by the location of the tallest plant within a footprint. For example, for terrain with constant slope s, the maximum possible value of ε_{z_{cb},z_w} is related to s and the footprint semi-major axis a by:

$$\max(\varepsilon_{z_{cb},z_w}) = \tan(s) \times a \quad (14)$$

However, $E(\varepsilon_{z_{cb},z_w})$ is zero if we assume that the location of the tallest plant within a footprint is random. So, Eq. (13) can be simplified as:

$$E(\varepsilon) = E(\varepsilon_{z_s,z_{max}}) + E(\varepsilon_{z_{max},z_{ct}}) + E(\varepsilon_{z_w,z_g}) \quad (15)$$

Furthermore, if the elevation of the detected signal start z_s matches the highest elevation z_{max} and the detected ground peak z_g matches

the mean ground elevation z_w, $E(\varepsilon_{z_s,z_{max}})$ and $E(\varepsilon_{z_w,z_g})$ can also be assumed to be zero. In such a situation, the mean error $E(\varepsilon)$ is solely determined by $\varepsilon_{z_{max},z_{ct}}$, the elevation difference of the maximum element z_{max} and canopy top z_{ct}:

$$E(\varepsilon) = E(\varepsilon_{z_{max},z_{ct}}) \quad (16)$$

It should be noted that z_{max} is always equal to or greater than z_{ct}, therefore, $E(\varepsilon_{z_{max},z_{ct}})$ can never be negative. This means that the direct method intrinsically tends to overestimate the canopy height when the signal start and mean ground elevation can be estimated with no bias.

The weighted mean ground elevation z_w was estimated by the optimal ground elevation metric z_g with a bias of 3.2 m, 0 m, and 3.7 m for the Mendocino, Santa Clara, and Lewis site, respectively (see Table 3). Therefore, $E(\varepsilon_{z_w,z_g})$ is −3.2 m, 0 m, and −3.7 m, respectively. According to the values of $E(\varepsilon_{z_s,z_{max}})$ from Table 4 and Eq. (15), it can be derived that $E(\varepsilon_{z_{max},z_{ct}})$ is 1.1 m, 3.8 m, and 3.8 m for the Mendocino, Santa Clara, and Lewis site, respectively. The positive values of $E(\varepsilon_{z_{max},z_{ct}})$ confirms the former analysis. Note that it is more likely to have positive $E(\varepsilon_{z_{max},z_{ct}})$ for sloped terrain with short and sparse canopy (see Fig. 1(e)). This explains why shots are located above the 1:1 line in the scatterplots of Fig. 5(b) when their canopy is short (h_a is less than 2 m) and canopy cover is low.

4.5.2. Multiple regression models

Table 6 lists the model fitting statistics at the three study sites calculated with five-fold cross validation. To compare models based on AIC, the common practice is to rescale the values with the minimum value of these models using $\Delta = AIC - AIC_{min}$, where AIC_{min} is the minimum of the different AIC values (Burnham & Anderson, 2002; Chen et al., 2007a). This transformation forces the best model to have $\Delta = 0$. Some simple rules are often useful in assessing the relative merits of models: Models with $\Delta \leq 2$ have substantial support, those in which $4 \leq \Delta \leq 7$ have considerably less support, and models with $\Delta > 10$ have essentially no support (Burnham & Anderson, 2002). In the following analysis, AIC is preferred for evaluating different models. However, adjusted R^2 and RMSE, along with the difference ε, are also analyzed since they have been widely used and are likely to be in continued use in the future (Anderson-Sprecher, 1994).

Among the three types of regression models, the DEM linear models produce the best results with adjusted R-square $R^2_{a\_cv}$ of 0.46, 0.34, and 0.24 for the Mendocino, Santa Clara, and Lewis site, respectively (Table 6). They also have the smallest AIC_cv and RMSE_cv values. This is reasonable given that the demExt is derived from airborne lidar data, which provides the most direct and precise information about terrain variability. Between the two edge-extent models, the nonlinear models have slightly lower AIC values than the linear models (Table 6). However, the AIC differences are less than 2 at these three sites. Therefore, the two edge-extent models are essentially the same at the individual site level.

4.5.3. Generalizability of the statistical models

4.5.3.1. Model generalizability at the inter-site level. The above cross-validation analysis at the individual sites indicated that the two edge-extent models have similar performance. However, when they are

Table 8
Edge-extent linear mixed-effects models developed at the inter-site level across the three study sites. Model 1 includes the random effects for both wfExt and leadExt+trailExt. Models 2 and 3 include the random effects only for wfExt and leadExt+trailExt, respectively. σ represents the standard deviation of the random effects, β is the estimate of the fixed effects, AIC is the model Akaike information criterion, and p-value is from the likelihood ratio test between the specific models (Model 2 or 3) and the general model (Model 1).

	Model 1	Model 2	Model 3
Random effects (σ)			
wfExt	0.23	0.18	-
leadExt + trailExt	0.08	-	0.31
Fixed effects (β)			
wfExt	0.69	0.72	0.80
leadExt + trailExt	−0.11	−0.16	−0.29
AIC	2663	2659	2672
p-value	-	0.74	0.00096

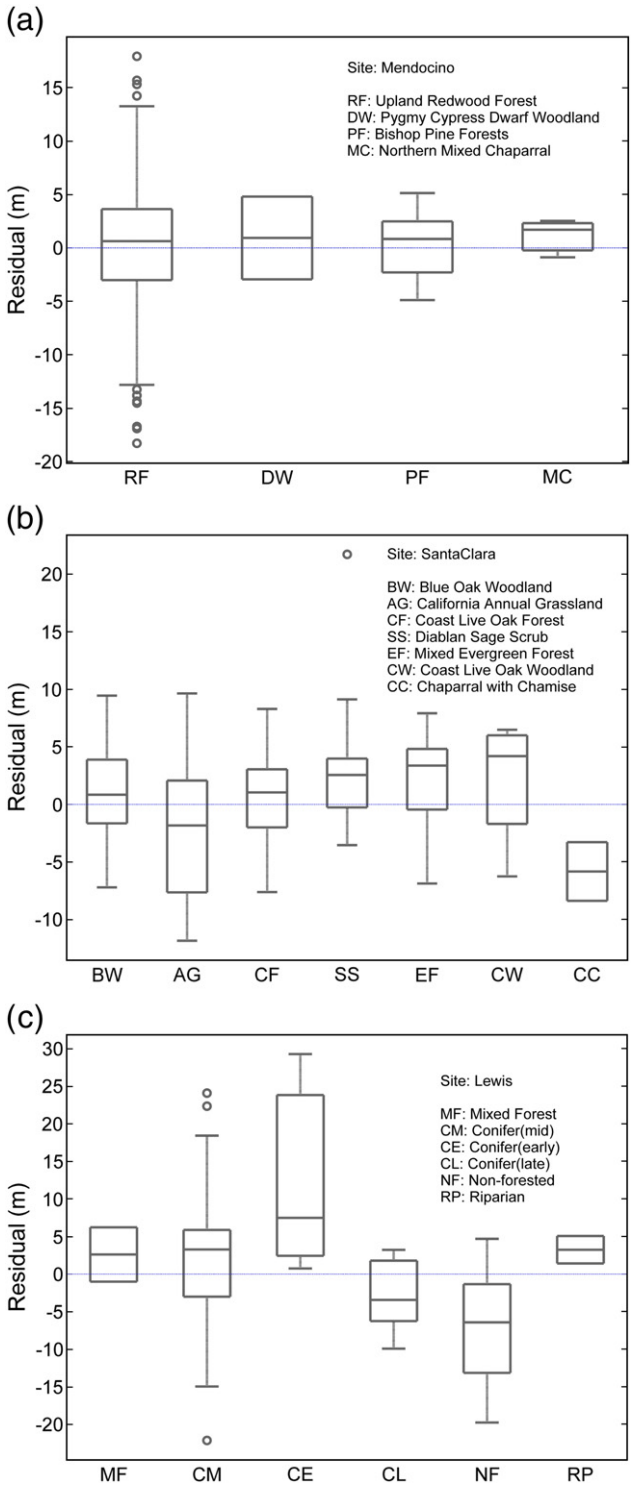

Fig. 7. Boxplots of the residuals of the fixed-effects edge-extent linear model for different vegetation community types at the (a) Mendocino, (b) Santa Clara, and (c) Lewis sites. Refer to Table 1 for detailed description of each vegetation community type or primary land cover.

applied across conifer and woodland sites, edge-extent linear models demonstrate better model generalizability and have smaller AIC and RMSE values than the edge-extent nonlinear models. For example, at the Santa Clara site, the AIC of the edge-extent nonlinear model (S_EN) is 6.8 smaller than the AIC of the edge-extent linear model (S_EL) (Table 7 and Fig. 6(e) and (f)). And the RMSE of model S_EN is 0.03 smaller than the one of model S_EL. However, when these two models are applied over the Mendocino site, the AIC of the linear model S_EL is 237.7 smaller than the AIC of the nonlinear model S_EN; the RMSE of the linear model S_EL is 17.14 m while the RMSE of the nonlinear model S_EN is 31.06 m, almost twice as large as the former (Table 7 and Fig. 6(b) and (c)).

The exploratory data analysis also reveals that the models have better generalizability between two conifer forest sites than between conifer and woodland sites (Table 7). For example, when the edge-extent linear model developed at the Lewis conifer site (L_EL) is applied at another conifer site in Mendocino, the AIC is only 20.6 larger than the AIC of the edge-extent linear model developed in Mendocino (M_EL), and the RMSE of model L_EL increases only by 0.30 m to 6.64 m compared to the RMSE (6.34 m) of model M_EL. However, when the edge-extent linear model developed at the woodland site (S_EL) is applied in Mendocino, the AIC is 398 larger than the one of model M_EL, and the RMSE of model S_EL is 17.14 m, which is almost three times of the RMSE (6.34 m) of model M_EL (Table 7 and Fig. 6(b)).

The following procedure is used to further rigorously test the generalizability of the edge-extent linear models at the inter-site level: first, three mixed-effects models were developed based on Eq. (10) (see Table 8). Model 1 is the general one with random effects for both wfExt and leadExt+trailExt. Models 2 and 3 are the specific ones with one of the random effects excluded. If the significance level of p-value from the likelihood ratio test between a specific model (Model 2 or 3) and the general model (Model 1) is less than 0.05, it implies that the random effects excluded in the specific model are statistically significant in the general model. The results show that the p-value for the random effects of wfExt is 0.00096 while the p-value for the random effects of leadExt+trailExt is 0.74 (see Table 8). So, there exist significant random effects for wfExt, which indicates that the fixed-effects edge-extent linear model (Eq. (5)) does not have the statistically-justified generalizability across the three sites. However, when the same procedure was applied to only the two conifer sites, it was found that neither of the random effects is statistically significant (results not reported) so the fixed-effects edge-extent linear model has the generalizability endorsed with the statistical test between the two conifer sites. This confirms the results from the previous exploratory data analysis. In the UMD Land Cover Classification Map (Hansen et al., 1998) generated from AVHRR imagery, the two conifer sites are within the same land cover while the woodland site is within a separate land cover. This implies that combining land cover maps from coarse-resolution remote sensing imagery such as AVHRR and MODIS with GLAS could improve estimates of maximum canopy height over large areas. Further research is desired to test this inference with more data.

Table 10
Inter-site analysis of the DEM linear model for predicting canopy height using simulated waveform metrics at 40 m and 10 m footprint sizes, respectively. ε, r, and RMSE are the difference, correlation, and root mean square error between predicted canopy height and the canopy height from airborne lidar data, respectively.

Model	Mendocino site			Santa Clara site			Lewis site		
	ε (m)	r	RMSE (m)	ε (m)	r	RMSE (m)	ε (m)	r	RMSE (m)
M40	−0.01	0.92	3.30	2.06	0.83	4.02	1.61	0.95	3.97
S40	−0.98	0.90	3.72	−0.13	0.85	3.16	0.51	0.95	3.74
L40	−1.55	0.92	3.69	0.82	0.84	3.36	−0.03	0.95	3.55
M10	0.04	0.99	1.39	1.13	0.97	1.72	0.37	0.99	1.28
S10	0.78	0.98	2.14	−0.01	0.98	1.01	1.28	0.99	1.85
L10	−0.40	0.98	1.66	0.23	0.98	1.10	−0.04	1.00	1.02

4.5.3.2. Model generalizability at the intra-site level. Generalizability of the edge-extent linear models was also tested using mixed-effects model at the intra-site level. The analysis unveiled that neither of the random effects is statistically significant for different vegetation community types within any of the three sites. In other words, the fixed-effects edge-extent linear models are adequate to model the maximum canopy height within individual sites. This is evident in the boxplots of the residuals of the fixed-effects edge-extent linear model for different vegetation community types at each site (Fig. 7). The boxes (representing upper and lower quartiles) of residuals of most vegetation community types do not depart from zero. The ones that depart from zeros mostly have a small number of shots (Table 1). Note that the vegetation community types of GLAS shots are from the Gap Analysis Program (GAP), which generates maps based on medium-resolution Landsat imagery. The results are encouraging because it implies that fine-scale vegetation community type maps are not needed to stratify maximum canopy height models based on GLAS data.

4.6. Simulations for the effects of footprint size on canopy height estimation

Tables 5 and 7 indicate that both direct and statistical methods suffer from very large RMSE. The most effective approach for improving model performance might be reducing the waveform footprint size. To examine the effects of footprint size on maximum canopy height estimation, simulations with the direct method and the

Table 9
Effects of footprint size on canopy height estimation based on waveform parameters simulated from airborne lidar data. ε, r, and RMSE are the difference, correlation, and root mean square error between predicted canopy height and the canopy height from airborne lidar data, respectively.

Site	Footprint size (m)	Direct method			DEM linear model			
		ε (m)	r	RMSE(m)	ε (m)	r	RMSE (m)	Model
Mendocino	40	1.22	0.91	3.67	−0.01	0.92	3.30	M40: $h = 0.97*\text{wfExt} - 0.52*\text{demExt}$
	30	0.62	0.94	2.92	−0.08	0.94	2.74	M30: $h = 0.97*\text{wfExt} - 0.46*\text{demExt}$
	20	0.19	0.97	2.18	−0.01	0.97	2.18	M20: $h = 0.96*\text{wfExt} - 0.35*\text{demExt}$
	10	0.10	0.99	1.40	0.04	0.99	1.39	M10: $h = 0.98*\text{wfExt} - 0.35*\text{demExt}$
Santa Clara	40	2.98	0.83	4.70	−0.17	0.85	3.19	S40: $h = 1.03*\text{wfExt} - 0.75*\text{demExt}$
	30	2.11	0.89	3.47	−0.04	0.90	2.52	S30: $h = 1.11*\text{wfExt} - 0.85*\text{demExt}$
	20	1.61	0.93	2.59	−0.07	0.94	1.89	S20: $h = 1.08*\text{wfExt} - 0.84*\text{demExt}$
	10	0.72	0.98	1.31	−0.01	0.98	1.01	S10: $h = 1.07*\text{wfExt} - 0.85*\text{demExt}$
Lewis	40	3.43	0.95	5.01	−0.03	0.95	3.55	L40: $h = 0.96*\text{wfExt} - 0.59*\text{demExt}$
	30	2.13	0.97	3.48	0.00	0.97	2.70	L30: $h = 0.97*\text{wfExt} - 0.54*\text{demExt}$
	20	1.24	0.98	2.36	−0.05	0.98	1.83	L20: $h = 0.99*\text{wfExt} - 0.62*\text{demExt}$
	10	0.45	0.99	1.25	−0.04	1.00	1.02	L10: $h = 1*\text{wfExt} - 0.64*\text{demExt}$

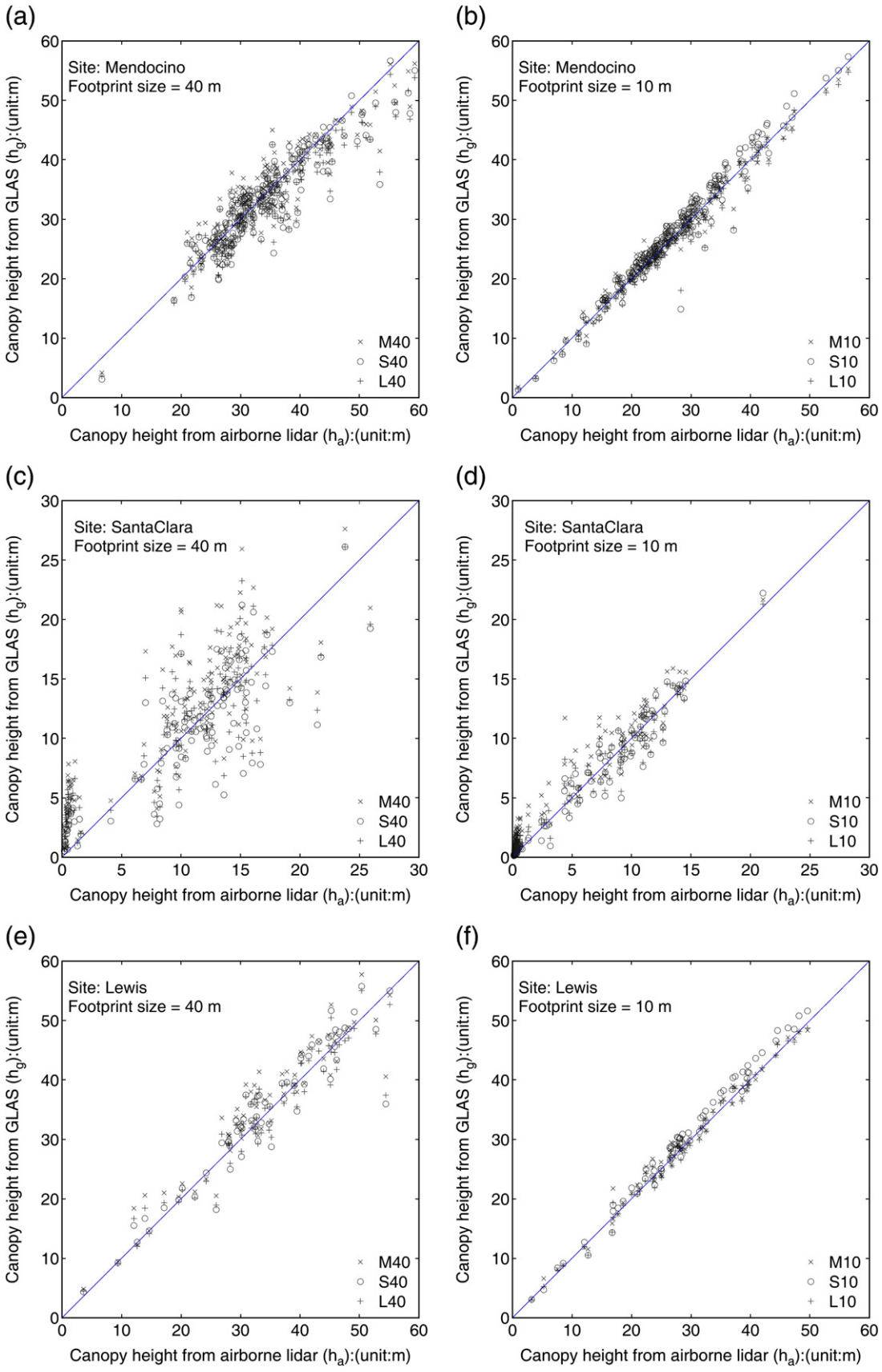

Fig. 8. Simulations of footprint size on canopy height estimation with the DEM linear models. The results from footprint sizes of 40 m (see subfigures (a), (c), and (e)) and 10 m (see subfigures (b), (d), and (f)) are shown for the three study sites ((a)-(b) for Mendocino, (c)-(d) for Santa Clara, (e)-(f) for Lewis).

DEM linear model were conducted at four footprint sizes varying from 40 m to 10 m by every 10 m.

It was found that the correlation coefficients r between the predicted canopy height and h_a get close to 1 and the RMSE reduces to 1–2 m when the footprint size decreases to 10 m for both direct and statistical methods (Table 9). For the direct methods, all difference ε values are positive, which agrees with the earlier conclusion that the direct methods tend to overestimate canopy height. Nevertheless, there is a positive relationship between footprint size and the difference ε. This means that smaller footprints can reduce the overestimation of canopy height for the direct methods. For the statistical methods, there is a clear pattern to show that the smaller the footprint size, the better the canopy height can be estimated with larger correlation coefficient and smaller RMSE (Table 9). The smaller footprint size can also increase the generalizability of the statistical model. The RMSE is about 50% lower for a footprint size of 10 m compared to the one for 40 m even when the models are applied across woodland and conifer sites (Table 10). This can be better visualized in Fig. 8 that shows the predicted canopy height versus h_a falls much closer around the 1:1 line for models from different sites when the footprint size reduces from 40 m to 10 m. All these analyses indicate that it is recommended that the footprint size of the next-generation satellite lidar systems be at least 10 m or so if we want to achieve meter-level accuracy of canopy height estimation using direct and statistical methods.

5. Conclusions

This study investigated the potential of GLAS for retrieving maximum canopy height over mountainous areas in the Pacific Coast region, including two conifers sites (one in California and the other in Washington) and one woodland site in California. Both direct and statistical methods were tested for canopy height estimation and it was found that:

- The direct methods tend to overestimate the maximum canopy height over mountainous sites based on the error budget analysis.
- The direct methods are complicated by the identification of waveform signal start and terrain ground elevation. There is no consistent optimal threshold that can be used for detecting waveform signal starts. Consistent with a previous study done in the Appalachians Mountain in North Carolina (Chen, 2010), the stronger one among the lowest two Gaussian peaks is the best ground elevation metric for the two conifer sites. However, at the woodland site, it is the strongest one among the lowest five Gaussian peaks that matches the ground elevation the best. This indicates that, if direct methods are used for estimating canopy maximum height, the ground elevation peaks over woodlands may need to be extracted separately from those over other land covers.
- The exploratory data analysis indicates that the edge-extent linear regression models have better generalizability than the edge-extent nonlinear models at the inter-site level.
- The inter-site level statistical test with mixed-effects models reveals that the edge-extent linear models have good generalizability between the two conifer sites but not between the conifer and woodland sites. The intra-site level statistical test indicates that the edge-extent linear models have good generalizability across different vegetation community types within any given site. These results unveil that the statistical modeling of maximum canopy height over large areas with edge-extent linear models only need to consider broad vegetation differences (such as woodlands versus conifer forests instead of different vegetation communities within woodlands or conifer forests).
- The simulation analysis indicated that the errors and uncertainty in canopy height estimation can be significantly reduced by decreasing the footprint size. When the footprint size is at 10 m, the canopy height bias and RMSE for the DEM linear model can be reduced to around 1 m and 1–2 m, respectively, even when the models are applied across woodland and conifer sites. This provides importance guidance in optimizing the footprint size of the next-generation satellite lidar systems for mapping canopy height over mountainous areas.

Despite these significant findings, this study can be improved in many aspects. For example, the airborne lidar point density is around 1 point per square meter, which may miss the treetops of some conifer trees. Using airborne lidar data with high point density may reduce the uncertainty of the analysis. Although it has been argued that airborne lidar can provide better accuracy than conventional field inventory (e.g., Hyyppä & Inkinen, 1999), it would be better if field data are available to support this. Another uncertainty is the time difference between airborne lidar data and GLAS data. Chen (2010) found that footprint size parameters supplied in the GLAS products might not be very accurate. Products with more accurate footprint sizes from the GLAS team will help identify the coincident airborne lidar data with better confidence. The variation of geolocation accuracy among campaigns also complicates the analysis. Although maximum canopy height focused in this study has important ecological applications, more research is needed to estimate other canopy heights such as the mean height, which may complement the maximum height for characterizing canopy structure.

Acknowledgements

Many thanks are extended to Dr. Guoqing Sun for explaining his senior-authored paper published in Remote Sensing of Environment (Sun et al., 2008). The airborne lidar data were acquired by Terrapoint under a contract to NASA, in collaboration with the U.S. Geological Survey, with funding from the NASA Solid Earth and Natural Hazards Program. I am also deeply indebted to the three anonymous reviewers for their constructive comments on improving the manuscript.

References

Anderson-Sprecher, R. (1994). Model comparisons and R^2. *American Statistician*, *48*, 113–117.

Baldocchi, D.D., Chen, Q., Chen, X., Ma, S., Miller, G., Ryu, Y., Xiao, J., Wenk, R., & Battles, J. (submitted). The dynamics of energy, water and carbon fluxes in a Blue Oak (*Quercus douglasii*) savanna in California, USA, In M.J. Hill & N.P. Hanan (Ed.), *Ecosystem Function in Global Savannas: Measurement and Modeling at Landscape to Global Scales*, CRC/Taylor and Francis.

Boudreau, J., Nelson, R., Margolis, H., Beaudoin, A., Guindon, L., & Kimes, D. (2008). Regional aboveground forest biomass using airborne and spaceborne LiDAR in Québec. *Remote Sensing of Environment*, *112*, 3876–3890.

Burnham, K. P., & Anderson, D. R. (2002). *Model selection and multimodel inference: A practical information-theoretic approach*, 2nd ed. New York: Springer-Verlag Press.

Chen, Q. (2007). Airborne lidar data processing and information extraction. *Photogrammetric Engineering & Remote Sensing*, *73*(2), 109–112.

Chen, Q. (2009). Improvement of the Edge-based Morphological (EM) method for lidar data filtering. *International Journal of Remote Sensing*, *30*(4), 1069–1074.

Chen, Q. (2010). Assessment of terrain elevation derived from satellite laser altimetry over mountainous forest areas using airborne lidar data. *ISPRS Journal of Photogrammetry and Remote Sensing*, *65*(1), 111–122.

Chen, Q., Gong, P., Baldocchi, D. D., & Tian, Y. (2007). Estimating basal area and stem volume for individual trees from LIDAR data. *Photogrammetric Engineering & Remote Sensing*, *73*(12), 1355–1365.

Chen, Q., Gong, P., Baldocchi, D. D., & Xie, G. (2007). Filtering airborne laser scanning data with morphological methods. *Engineering & Remote Sensing*, *73*(2), 175–185.

Duncanson, L., Niemann, K. O., & Wulder, M. A. (2010). Estimating forest canopy height and terrain relief from GLAS waveform metrics. *Remote Sensing of Environment*, *114*(1), 138–154.

Duong, V. H., Lindenbergh, R., Pfeifer, N., & Vosselman, G. (2008). Single and two epoch analysis of ICESat full waveform data over forested areas. *International Journal of Remote Sensing*, *29*(5), 1453–1473.

Hansen, M., DeFries, R., Townshend, J. R. G., & Sohlberg, R. (1998). UMD Global Land Cover Classification, 1 Kilometer, 1.0. *Department of Geography* (pp. 1981–1994). Maryland: University of Maryland, College Park.

Harding, D.J. (2004). TerraPoint LIDAR mapping instrumentation and methodology. http://core2.gsfc.nasa.gov/lidar/terrapoint/TerraPoint_System_Description.pdf (accessed on March 21, 2009).

Harding, D. J., & Carabajal, C. C. (2005). ICESat waveform measurements of within-footprint topographic relief and vegetation vertical structure. *Geophysical Research Letters*, *32*(L21S10). doi:10.1029/2005GL023471.

Hofton, M. A., Minster, J. B., & Blair, J. B. (2000). Decomposition of laser altimeter waveforms. *IEEE Transactions on Geoscience and Remote Sensing*, *38*(4), 1989−1996.

Hyde, P., Dubayah, R., Peterson, B., Blair, J. B., Hofton, M., Hunsaker, C., et al. (2005). Mapping forest structure for wildlife habitat analysis using waveform lidar: Validation of montane ecosystems. *Remote Sensing of Environment*, *96*(3–4), 427−437.

Hyyppä, J., & Inkinen, M. (1999). Detecting and estimating attributes for single trees using laser scanner. *The Photogrammetric Journal of Finland*, *16*(2), 27−42.

Kvålseth, T. O. (1985). Cautionary note about R^2. *American Statistician*, *39*, 279−285.

Lefsky, M. A., Harding, D. J., Keller, M., Cohen, W. B., Carabajal, C. C., Del Bom Espirito-Santo, F., et al. (2005). Estimates of forest canopy height and aboveground biomass using ICESat. *Geophysical Research Letters*, *32*(L22S02). doi:10.1029/2005GL023971.

Lefsky, M. A., Keller, M., Pang, Y., de Camargo, P. B., & Hunter, M. O. (2007). Revised method for forest canopy height estimation from Geoscience laser Altimeter System waveforms. *Journal of Applied Remote Sensing*, *1*, 1−18.

Moles, A. T., Warton, D. I., Warman, L., Swenson, N. G., Laffan, S. W., Zanne, A. E., et al. (2009). Global patterns in plant height. *Journal of Ecology*, *97*(5), 923−932. doi:10.1111/j.1365-2745.2009.01526.x.

Nelson, R. (in press). Model effects on GLAS-based regional estimates of forest biomass and carbon. International Journal of Remote Sensing, Special Issue: Silvilaser 2008.

Neuenschwander, A. L., Urban, T. J., Gutierrez, R., & Schutz, B. E. (2008). Characterization of ICESat/GLAS waveforms over terrestrial ecosystems: Implications for vegetation mapping. *Journal of Geophysical Research*, *113*(G02S03). doi:10.1029/2007JG000557.

Pang, Y., Lefsky, M., Andersen, H., Miller, M. E., & Sherrill, K. (2008). Validation of the ICEsat vegetation product using crown-area-weighted mean height derived using crown delineation with discrete return lidar data. *Canadian Journal of Remote Sensing*, *34*(Suppl. 2), S471−S484.

Rosette, J. A. B., North, P. R. J., & Suarez, J. C. (2008). Vegetation height estimates for a mixed temperate forest using satellite laser altimetry. *International Journal of Remote Sensing*, *29*(5), 1475−1493.

Sharpe, G. W., Sharpe, W., & Hendee, J. C. (2003). *Introduction to forests and renewable resources* (pp. 51−84). New York: McGraw Hill.

Sun, G., Ranson, K. J., Kimes, D. S., Blair, J. B., & Kovacs, K. (2008). Forest vertical structure from GLAS: An evaluation using LVIS and SRTM data. *Remote Sensing of Environment*, *112*(1), 107−117.

Westoby, M., Falster, D. S., Moles, A. T., Vesk, P. A., & Wright, I. J. (2002). Plant ecological strategies: Some leading dimensions of variation between species. *Annual Review of Ecology & Systematics*, *33*, 125−159.

Zwally, H. J., Schutz, B., Abdalati, W., Abshire, J., Bentley, C., Brenner, A., et al. (2002). ICESat's laser measurements of polar ice, atmosphere, ocean, and land. *Journal of Geodynamics*, *34*, 405−445.